



## Decadal-scale variability of sardine and anchovy simulated with an end-to-end coupled model of the Canary Current ecosystem

J.C. Sánchez-Garrido<sup>a,\*</sup>, F.E. Werner<sup>b</sup>, J. Fiechter<sup>c</sup>, K.A. Rose<sup>d</sup>, E.N. Curchitser<sup>e</sup>, A. Ramos<sup>f</sup>, J. García Lafuente<sup>a</sup>, J. Arístegui<sup>g</sup>, S. Hernández-León<sup>g</sup>, A. Rodríguez Santana<sup>f</sup>

<sup>a</sup> Physical Oceanography Group, University of Malaga, Campus de Teatinos s/n, 29071 Malaga, Spain

<sup>b</sup> NOAA Fisheries, 1315 East-West Highway, Silver Spring, MD 20910, USA

<sup>c</sup> Institute of Marine Sciences, University of California, Santa Cruz, CA 95064, USA

<sup>d</sup> University of Maryland Center for Environmental Science, Horn Point Laboratory, PO Box 775, Cambridge, MD 21613, USA

<sup>e</sup> Department of Environmental Sciences, Rutgers University, 14 College Farm Road, New Brunswick, NJ 08901, USA

<sup>f</sup> Fac. Ciencias del Mar, Univ. Las Palmas de Gran Canaria, 35017 Las Palmas, Spain

<sup>g</sup> Instituto de Oceanografía y Cambio Global (IOcAG), Univ. Las Palmas de Gran Canaria, 35017 Las Palmas, Spain

### ABSTRACT

Small pelagic fish species, such as sardine and anchovy, can exhibit dramatic decadal-scale shifts in abundance in response to climate variability. Understanding the mechanisms and the relationships among the different components of the food web through which environmental forcing can drive the observed fish variability remains a challenging problem. The modelling study described herein, focusing on the Canary Current System, implements and builds on earlier modelling efforts by Rose et al. (2015) and Fiechter et al. (2015) in the California Current System. This new application of the modelling framework to the Canary Current system provides an approach that bridges a comprehensive database with end-to-end (climate-to-fish) modelling, thereby enabling the investigation of the sources of variability of sardine (*Sardina pilchardus*) and anchovy (*Engraulis encrasicolus*). The aim of the modelling effort is to gain insights into the underlying mechanisms that drive the observed biological variability. Particular attention is given to the absence of regime shifts between sardine and anchovy in the Canary Current, which is a distinctive feature among the four major eastern boundary upwelling ecosystems. A model simulation for 1958–2007 was performed and analysed. The biological traits and behaviours prescribed for sardine and anchovy for the Canary Current give rise to different spatial distribution of their populations, and in contrast with other eastern boundary upwelling ecosystems, to synchronous (rather than asynchronous) variability of their abundance and biomass. Analyses of years with anomalously high increases and declines of the adult populations implicate food availability (instead of temperature or other environmental drivers) as the main factor determining recruitment for both sardine (via spawning and survival of feeding age-0 individuals) and anchovy (via survival of feeding age-0 individuals). The common dependence of sardine and anchovy on food, together with the domain-wide response of zooplankton to climate forcing generated in the model, provides a plausible explanation for the synchronization of the two populations. Our results also point at differences between sardine and anchovy; while the two species thrive under enhanced upwelling-favourable winds, anchovy larvae become particularly vulnerable to drift mortality, and thus do better than sardine under more moderate upwelling conditions.

### 1. Introduction

Small pelagic fish, such as sardines, anchovies, and herrings, account for about one half of the global marine food catch (Fréon et al., 2005). They are most abundant in major upwelling regions where they sustain major world's fisheries and play a crucial ecological role linking plankton and top predators. In these upwelling regions, the biomass of small pelagic fish is frequently dominated by sardine and anchovy, and is characterized by dramatic decadal-scale fluctuations (or “boom-bust” cycles) in their population abundances (Bakun, 1996; Alheit et al., 2009). Evidence for such fluctuations can be found in paleoecological records (e.g., Baumgartner et al., 1992; Salvatelli et al., 2018), suggesting that they are primarily controlled by climate variability and

only in part by fishing pressure. Sustained research efforts have been conducted to determine the linkages between changes in environmental conditions and the interannual variability in small pelagic fish populations (Checkley et al., 2010). However, the underlying mechanisms are not yet fully understood, and aspects of the response of small pelagic fish to projected changes in climate remain an active area of research.

The population dynamics of small pelagic fish, particularly sardines and anchovies, have received special attention in major boundary currents (Fréon et al., 2009), where catches of the two species have appeared in alternating cycles (e.g., Lluch-Belda et al., 1989; Schwartzlose et al., 1999; Takasuka et al., 2008). Strikingly, the populations of small pelagics in different systems (i.e., different oceanic

\* Corresponding author.

E-mail address: [jcsanchez@ctima.uma.es](mailto:jcsanchez@ctima.uma.es) (J.C. Sánchez-Garrido).

<https://doi.org/10.1016/j.pocean.2018.12.009>

Received 19 February 2018; Received in revised form 3 December 2018; Accepted 13 December 2018

Available online 18 December 2018

0079-6611/ © 2018 Elsevier Ltd. All rights reserved.

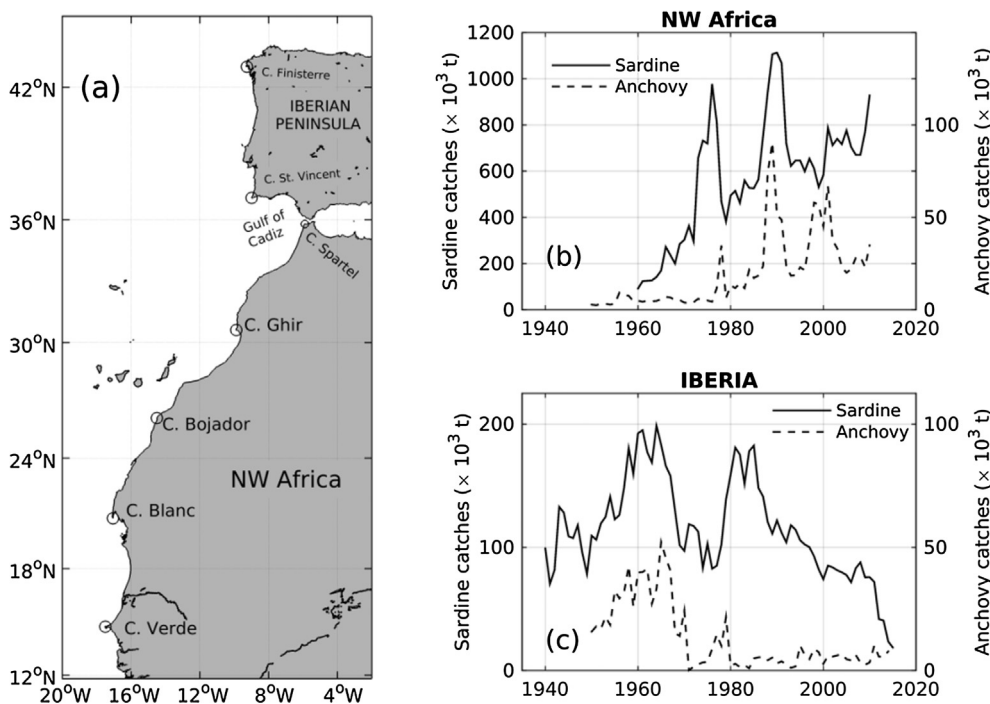


Fig. 1. (a) Physical domain of the CanCS with locations referred in the text. (b) Historical sardine (*S. pilchardus*) and anchovy (*E. encrasicolus*) landings estimates in NW Africa. (c) Same as panel (b) for Western Iberia. Landings were retrieved from FAO (2001, 2012; NW Africa sardine landings), SeaAroundUs database (<http://www.seaaroundus.org/>; NW Africa anchovy landings), ICES (2016a; Iberian sardine landings, ICES division 9a), and ICES (2016b; Iberian anchovy landings).

basins), appear to oscillate in synchrony, suggesting a global bottom-up role of climate teleconnection patterns. For example, sardine and anchovy in the California Current appear to fluctuate in synchrony with their counterparts in the Humboldt Current. In the Atlantic, sardine and anchovy in the Benguela Current have also varied synchronously, although in opposite phase with the California Current and Humboldt (Pacific) populations. In contrast, in the Canary Current System (CanCS), no regime shifts or dominant sardine and anchovy cycles have been reported. In this sense, the CanCS is distinct among eastern boundary upwelling systems, as sardine abundance is permanently dominant over that of anchovy and the two species vary nearly in phase as suggested by landings records (Fig. 1). A number of explanations have been proposed for the dominance of sardine as well as for their documented fluctuations (Aristegui et al., 2009), but hypotheses are particularly difficult to test in the CanCS because of the absence of systematic observations across the region, particularly off NW Africa (Aristegui et al., 2009). This circumstance largely constrains our understanding – even description – of the CanCS small pelagic fish variability and fisheries.

While data collection is still an ongoing challenge, ecosystem models are becoming more inclusive of additional processes and their interactions, enabling exploration and assessment of driving mechanisms. A demonstration of this development are end-to-end models that typically combine ocean circulation models with lower- and higher-trophic level components in a single modelling framework (Travers et al., 2007; Rose et al., 2010). The use of end-to-end models for forecasting purposes is still in development, but they have been proven to be valuable tools for testing hypotheses and gaining new insights into the response of small pelagic fish species to climate variability. A fully-coupled, three-dimensional example is the individual-based model for sardine and anchovy developed by Rose et al. (2015; hereafter R15), whose potential was recently demonstrated with a 50-year historical simulation of the California Current ecosystem. Other related approaches (Travers et al., 2007; Fulton, 2010) include the Atlantis modelling system (Fulton et al., 2011) and a recent model by Brochier et al. (2018).

The R15 model generated decadal-scale variability of sardine and anchovy biomass that was qualitatively similar to the observed variability. In a more detailed analysis, Fiechter et al. (2015) analysed the

same simulation and identified the environmental factors controlling the interannual variability in population dynamics and showed that sardine and anchovy were sensitive to different environmental conditions. The variability of adult sardine was associated with temperature and survival of age-0 individuals, while fluctuations of anchovy primarily depended on availability of food and age-1 growth. Based on the model simulation, they inferred that ocean temperature and food (plankton) typically vary in opposite phase, and thus provide a possible underlying mechanism for the alternating cycles between sardine and anchovy in the California Current observed during the 20th century. Linkages between the variability of the sardine and anchovy populations and the most relevant modes of climate variability in the region (e.g., the Pacific Decadal Oscillation and El Niño Southern Oscillation) were quantified using correlation analyses.

In the present paper, we adapt the R15 model to the CanCS. The objective of this paper is threefold. First, to demonstrate that the R15 model can be applied to perform multi-decadal simulations in other ecosystems with moderate adaptations. In particular, we examine the ability of the R15 model to reproduce synchronous decadal-scale variability of sardine and anchovy in the CanCS, a unique behaviour among major eastern boundary upwelling ecosystems. Second, identify the primary biological and environmental drivers of sardine and anchovy oscillations within the historical simulation. Lastly, our goal is also to identify fundamental differences relative to the population dynamics found for sardine and anchovy in the California Current using the same R15 modelling approach (Fiechter et al., 2015). The organization of this paper is as follows. Section 2 briefly reviews the main physical features of the CanCS, including the documented interannual variability of sardine and anchovy in the region. Section 3 describes the components of the R15 end-to-end model and the configuration specific to the present CanCS application. Results of a 50-year historical simulation (1958–2007) are described in Section 4 and 5; with Section 6 offering detailed analyses to identify the mechanisms for the simulated variability. Finally, Section 7 includes a summary and discussion of the results.

## 2. Overview of the Canary Current

### 2.1. Subregions and physical features

The CanCS extends roughly from the northwestern tip of the Iberian Peninsula in the north to Cape Verde in the south (Fig. 1a; Barton, 1998; Aristegui et al., 2006). The system comprises several ocean currents, hosts different water masses, and is characterized by irregular shorelines, variable bottom topographies, and uneven wind regimes. Three different regions can be distinguished: the Iberian sub-region in the north (Cape Finisterre–Strait of Gibraltar), a central region between the Strait of Gibraltar and Cape Blanc (Morocco–Sahara), and a southern sub-region between Cape Blanc and Cape Verde (Mauritania–Senegal). Upwelling favourable conditions occur year-round between Cape Blanc and Cape Ghir in the central region, and only seasonally in the northern (spring–summer) and southern (fall and winter) parts, resulting from meridional oscillations of the Trade winds. Moving from north to south, the transition between the northern and central regions is marked by the presence of the Gulf of Cadiz, where the shoreline loses its prevailing north-to-south orientation and becomes less prone for wind-driven upwelling to occur. This turning point in the shoreline prevents a clear connection between the Portugal Current off the Iberian Peninsula, particularly apparent in the summer, and the Canary Current, the main wind-driven current along NW Africa. Further south, the transition between the central and southernmost regions around Cape Blanc is marked by the presence of a density front that separates North Atlantic Central Water in the north from South Atlantic Central Water to the south; the latter being slightly cooler, fresher, and richer in nutrients.

### 2.2. Sardine and anchovy

#### 2.2.1. Biological traits and behaviours

The European sardine (*Sardina pilchardus*) and the European anchovy (*Engraulis encrasicolus*) are present all along the CanCS. These species share a number of general traits common to other sardine and anchovy species (Garrido and van der Lingen, 2014; Checkley et al., 2017). Both species are short-lived, highly fecund, spawn in batches and have opportunistic life histories typical of small pelagic fish species (Blaxter and Hunter, 1982; Winemiller and Rose, 1992). Sardine and anchovy have both capital and income breeding characteristics, and their egg production is greatly affected by the body condition of spawners (Ganias et al., 2014).

Like other sardine and anchovy, European anchovy and sardine also differ from each other in two fundamental traits related to their feeding and their migratory behaviour. Both sardine and anchovy eat primarily zooplankton, but can also eat phytoplankton and fish eggs. However, sardine feed mainly by filtering particles from water (filter feeders), while anchovy filter and bite individual particles (particulate feeders). Moreover, anchovy possess coarser gill rakers than sardine that reflects a greater affinity to feed on larger prey. Another significant difference lies in their ability to swim. Sardine are better swimmers than anchovies and as such are able to migrate longer distances.

Some biological traits of sardine and anchovy are specific to the CanCS ecosystem. Here, sardine spawn from autumn to spring (Coombs et al., 2006; Ganias et al., 2014), while anchovy spawn from spring to autumn. In Atlantic waters, the spawning seasonality of anchovy has been studied in detail in the Gulf of Cadiz (Millan, 1999; Bernal et al., 2011) and in the Bay of Biscay (Motos, 1996), but little is known about the NW Africa populations. Ambient temperatures affect the reproductive seasonality of both species, and hence the timing and duration of the spawning season can slightly change from one habitat to another. Off NW Africa, observed spawning temperatures for sardine range between 15 and 20 °C (Coombs et al., 2006). For anchovy, we are not aware of documented spawning temperatures in this region. Sardine tend to remain close to the coast but can be found as far offshore as

the Canary, Madeira, and even the Azores Archipelago (Barange et al., 2009), while anchovy is largely restricted to the continental shelf. Sardine live up to 10 years with a maximum length of about 240 mm. Anchovy are shorter-lived (about 4–5 years) and are smaller at age (150 mm maximum length) than sardine. A distinctive behaviour of the European sardine is that it shows less pronounced migration patterns than other sardine species (Alheit, 2009).

#### 2.2.2. Variability of sardine and anchovy

Based on landings, the European sardine is the most dominant small pelagic fish of the CanCS. The only exception to this dominance is found to the south of Cape Bojador where *Sardinella* species (*Sardinella aurita* and *Sardinella maderensis*) become as, or more, abundant than sardine (Brochier et al., 2018). The largest population resides off Morocco–Sahara with a total estimated biomass of up to 5 million tonnes (Mt; Barange et al., 2009). This biomass is mainly distributed in three important fishing areas that have been traditionally associated with different stocks (Belvêze and Erzini, 1983; Kifani, 1998), although seasonal interactions and mixing of the subpopulations have been suggested (Bravo de Laguna et al., 1976). The boundaries of the assumed stocks are roughly in Cape Bojador and Cape Ghir. Off of Iberia, the sardine biomass is estimated to be 0.5 Mt.

Decadal-scale variability of sardine biomass is reflected in the records of annual catches (solid line in Fig. 1b). Total catches off Morocco–Sahara have shown a positive trend since the beginning of the industrial exploitation of the stocks in the late 1950's. Maximum annual catches (approximately 1 Mt) were recorded during the mid-1970's and early 1990's. There is also evidence for shifts in the populations' distribution (see Aristegui et al., 2009). A well-documented case is the southward shift of the boundary between sardine and sardinella in the late 1960's. The sardine population extended to the south of Cape Blanc and its fisheries notably increased from Cape Verde to Cape Bojador during the 1970's, while the central and northern stocks, which provided the bulk of catches until then, declined. This southward shift of the sardine was attributed to a strengthening of the upwelling intensity off Western Sahara (Holzlöhner, 1975; Binet, 1988) and a concomitant weakening of upwelling around Cape Ghir (Belvêze and Erzini, 1983). A second southward shift of the sardine population took place during the late 1980's. Off Iberia, long term variability of biomass is also evident in the records (solid line in Fig. 1c). The historical maximum of landings took place in the mid 1960's (190–200 kt; ICES, 2016a). Landings then decreased until the mid-1970's (80–90 kt), and recovered again to reach a second maximum during the mid-1980's (180 kt). Since then, the Iberian sardine fisheries have been in decline, with landings of only 18 kt in 2015.

Anchovy is present off NW Africa although little is known about the biology of this species in the region, perhaps because of the relative small size of its fisheries. Anchovy catches are about one order of magnitude smaller than sardine catches (Fig. 1b; dashed line). Anchovy occur persistently in the Gulf of Cadiz, a recognized spawning and nursery ground, and are less common along the Portuguese and the northwestern Spanish coasts. Decadal-scale variability of anchovy biomass is also suggested in the historical landing estimates off NW Africa and Iberia (Fig. 1b and c), which are positively correlated with the sardine's ( $r = 0.64$  and  $r = 0.55$  in NW Africa and Iberia respectively). This fact represents a qualitative difference with respect to other major boundary current ecosystems, particularly the California Current, in which sardine and anchovy catches and their respective biomass estimates vary asynchronously (Schwartzlose et al., 1999; R15). The lack of observations in the CanCS raises the question whether catches reflect actual fish biomass. The positive tendency of NW Africa catches is very likely the consequence of increasing fishing effort by industrial fleets, which emerged in 1973 and developed rapidly until the mid 90's (Baddy and Guénette, 2002), and does not seem to be connected with a long-term growth of the populations. Likewise, the prolonged decline of the Iberian fisheries after the early 1980's seems tightly related to

overexploitation of the stock. For similar reasons, because fishing pressure off NW Africa has increased quite linearly over time (Baddy and Guénette, 2002), major oscillations in landings are mainly ascribed to the natural variability of the ecosystem. The interplay between anthropogenic forcing (i.e., fishing mortality) and the fish population dynamics is complex, however, and the above interpretations should be taken with caution. Bearing in mind these caveats, historical landings in the CanCS differ qualitatively from those in other eastern boundary current systems (also subject to uncertainties), suggesting a positive correlation between sardine and anchovy populations. We refer to this behaviour to as synchronous variation (as opposed to asynchronous variation employed in other ecosystems), but note that the correlation – or synchrony – between sardine and anchovy landings is obviously not perfect.

### 3. End-to-end ecosystem model

The end-to-end model combines a primitive-equation ocean circulation model, a lower trophic level sub-model for nutrient, phytoplankton and zooplankton (NPZ), and an individual-based model (IBM) for the population dynamics of sardine and anchovy. We performed a 50-year historical run of the period 1958–2007 to allow for decadal-scale variability of fish biomass to be generated in the model. The simulation was completed after 12 days running on 32 CPUs of an Intel E5-2670 cluster. The configuration and initialization of each model component as well as the coupling between them is described next.

#### 3.1. Ocean circulation model

The Regional Ocean Modelling System (ROMS; Shchepetkin and McWilliams, 2005) was employed. ROMS is a free-surface primitive-equation model that uses a mode-splitting time stepping and terrain-following vertical coordinates. The present configuration for the CanCS roughly covers the domain 7.5°N to 50°N and 38°W to 1°W with a horizontal resolution of 12 km and 38  $\sigma$ -levels (Fig. 2). Such horizontal resolution allows for the generation of some mesoscale variability in the model. A curvilinear grid aligned with the mean coastline orientation was used in order to maximize the ratio between ocean and land cells. This configuration is similar to the CanCS application of Mason et al. (2011) but with lower resolution in the horizontal and slightly greater resolution in the vertical. The bathymetry was extracted from the ETOPO1 database (Amante and Eakins, 2009) and smoothed in order to

reduce large bottom topography slopes that can lead to spurious pressure gradients in ROMS. The model was run with a horizontal eddy viscosity and diffusivity of  $5 \text{ m}^2 \text{ s}^{-1}$ . Such small coefficient was chosen because both momentum and tracers were advected with a third-order upstream scheme that introduces additional (numerical) dissipation. In the vertical, the nonlocal K-profile turbulence parameterization (Large et al., 1994) was applied, whereas advection was computed according to a fourth-order centred scheme.

Boundary and initial values were derived from monthly outputs of the Simple Ocean Data Assimilation reanalysis (SODA 2.0.2; Carton and Giese, 2008). For the barotropic mode, we applied the Flather (1976) boundary condition combined with the radiation condition of Chapman (1985) for the sea surface height. For the baroclinic mode, a simple clamped condition was used for both momentum and tracers. In addition, a nudging “sponge” layer of the 30 grid points adjacent to the open boundaries was introduced in order to minimize spurious signals that could otherwise be generated along boundary regions. Fields were nudged to climatological values with a nudging coefficient varying linearly from  $1/5 \text{ days}^{-1}$  in the outer part of the sponge layer to  $1/120 \text{ days}^{-1}$  in its inner part. The Strait of Gibraltar was represented by three model grid cells with a sill at 340 m depth. This configuration is a compromise between realism of simulated exchange flow between the Atlantic and the Mediterranean Sea and the use of sufficiently gentle bottom topography to guarantee the model stability. The simulated exchange transport was  $1.2 \text{ Sv}$ , which is somewhat larger than recent estimates ( $0.85 \text{ Sv}$ ; Sammartino et al., 2015).

Atmospheric forcing was derived from data of the Common Ocean- Ice Reference Experiments (CORE2; Large and Yeager, 2008) and consists of 6-hourly winds, air temperature, sea level pressure and specific humidity, daily short-wave and downward long-wave radiation, and monthly precipitation. From these inputs, surface momentum flux, sensible and latent heat fluxes, and upward long-wave radiation were interactively computed by the model using a standard bulk formula. Fresh water fluxes from river discharges were not included in the model.

#### 3.2. Lower trophic NPZ model

The lower trophic model NEMURO (Kishi et al., 2007) was used. NEMURO is a NPZ model that has been applied to a variety of ecosystems (Werner et al., 2007; Kishi et al., 2011). The present version of NEMURO is the same as described by R15. Modifications with respect

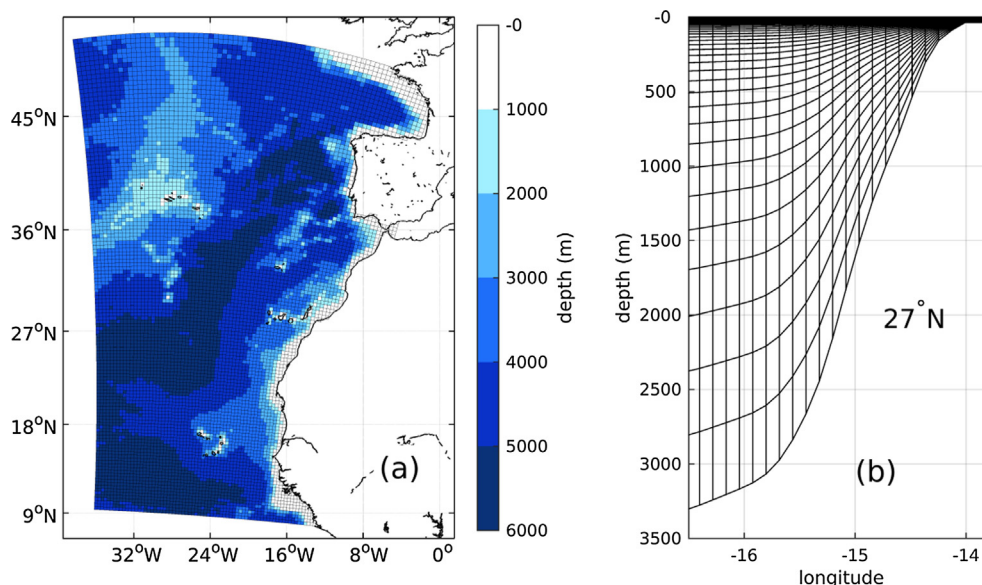


Fig. 2. (a) Model grid and bathymetry. For clarity, only one of every three grid lines is shown. (b) Vertical discretization over the continental slope along 27°N.

to the standard code of Kishi et al. (2007) include the light limitation for photosynthesis proposed by Platt et al. (1980), and zooplankton mortality due to consumption by fish (Megrey et al., 2007). NEMURO incorporates 11 state variables: nitrate, ammonium, silicic acid, small phytoplankton (PS), large phytoplankton (PL), small zooplankton (ZS), large zooplankton (ZL), predatory zooplankton (ZP), particulate organic nitrogen, dissolved organic nitrogen, and particulate organic silicon. Advection and mixing of these tracers is done in ROMS using the same numerical schemes as for temperature and salinity.

Initial and boundary conditions for nitrate and silicic acid were derived from the global monthly climatology of Conkright and Boyer (2002). Conditions for ammonium, phytoplankton, zooplankton and detritus were set to a small constant value (0.1 mmol N m<sup>-3</sup>). The NEMURO parameters were initially set as in R15 motivated by the similarity of their application to an upwelling system. After this, maximum photosynthetic rates, half saturation constants of phytoplankton, and initial slope of the photosynthesis-light curves were adjusted to achieve realistic chlorophyll (*chl*) and nutrient concentration and patterns for the CanCS. Zooplankton parameters remained fixed at R15 values during the calibration and were used for the historical simulation.

The resulting phytoplankton-related parameter values differed only slightly from those used in R15, except for a major difference regarding silicic acid. In NEMURO, silicic acid is consumed by the large phytoplankton group (PL) which therefore represents a diatom-like organism. Introduction of silicic acid as a possible limiting nutrient is required in ecosystems in which blooms are largely associated with the presence of diatoms. In our calibration for the CanCS, the prescription of a finite half saturation constant for silicic acid,  $K_{Si}$ , and therefore its inclusion as a possible limiting nutrient for PL, results in a substantial underestimation of chlorophyll concentration (*chl*) off NW Africa. Observations (Aristegui et al., 2004; García-Muñoz et al., 2005) do not reveal a clear dominance of diatoms in the upwelling region off NW Africa – large flagellates being most abundant. While the inclusion of a diatom-like organism in the model can locally improve *chl* patterns, for example north of 45°N during the north Atlantic spring bloom, the most satisfactory overall result is achieved when suppressing silicic acid limitation ( $K_{Si} = 0$ ). The photoinhibition coefficient was also given the same value for PS and PL ( $\beta = 4.5 \times 10^{-4} \text{ W}^{-1} \text{ m}^2 \text{ d}^{-1}$ ). The rest of the phytoplankton (and all of the zooplankton) parameters were as in R15.

### 3.3. Fish individual based model (IBM)

#### 3.3.1. Description

The IBM simulates sardine, anchovy and a generic fish predator species introduced to impose dynamical mortality on sardine and anchovy. The model is described in detail in R15. Only the movement and consumption rates of predatory super-individuals were simulated (not the population dynamics). Individuals of all three species were tracked within the same three-dimensional grid used by ROMS and NEMURO, and their positions were updated every hour. The model employs the super-individual approach introduced by Scheffer et al. (1995), in which a fish population is represented by a number of fixed individuals (super-individuals). Each super-individual represents a number of identical population individuals, referred to as the super-individuals' worth. By changing the super-individuals' worth (decrease due to mortality), and not the number of super-individuals themselves, changes of the population as a whole can be simulated using a fixed number of model individuals. In this manner, an actual population of millions of individuals can be represented with a known number of super-individuals and affordable computer memory.

The life cycle of sardine and anchovy in the IBM was defined by egg, yolk-sac larvae, larval, juvenile, and adult stages. Adults, in turn, comprise sub-adult and sexually mature individuals. Ambient temperature (at the location of each individual) determined the development of eggs and yolk-sac larvae. Eggs hatched into yolk-sac larvae and

yolk-sac larvae became larvae with a given initial weight and length ( $1.53 \times 10^{-3} \text{ g}$  and 6 mm for sardine;  $8.75 \times 10^{-5} \text{ g}$  and 4.3 mm for anchovy). Following Zweifel and Lasker (1976), these transformations occurred at the time in which the hourly cumulative value of

$$D_T = \frac{a_1 e^{a_2(1-e^{-a_3 T})}}{\ln\left(\frac{d_1}{d_1 - \ln\left(\frac{d_2}{d_3}\right)}\right)} \quad (1)$$

exceeded unity. In the above,  $T$  is the sea water temperature at the individuals' location (updated hourly) and the rest of the coefficients (different for eggs and yolk-sac larvae) are parameters that determine the rate of development a function of temperature. Metamorphosis from larvae to juveniles and maturation were dependent on fish length: sardine and anchovy larvae became juvenile at 35 mm for both species and sub-adults reached sexual maturity at 152 mm for sardine and at 115 mm for anchovy (Belvèze et al., 1980; ICES, 2017). The transition from juveniles to sub-adults occurred automatically on January 1 of each year. Individuals were further classified according to their age. Starting from age-0, the age class of a given individual was updated every January 1 regardless of its actual birthday.

Growth in weight of each sardine and anchovy super-individual depended on consumption, respiration, and energy loss due to reproduction, and was computed each hour from bioenergetics and a functional response relationship using temperature and zooplankton concentration generated from ROMS and NEMURO. Realized consumption ( $C$ ) was calculated as (Rose et al., 1999a, 1999b):

$$C = \sum_{j=1}^3 C_j; \quad C_j = \frac{C_m W \left(\frac{Z_j V_{sj}}{K_{sj}}\right)}{1 + \sum_{k=1}^3 \left(\frac{Z_k V_{sk}}{K_{sk}}\right)} \quad (2)$$

where  $C_j$  is the consumption rate by a fish on prey  $j = 1, 2, 3$  (corresponding to the three zooplankton types ZS, ZL, ZP);  $C_m$  is the maximum consumption rate dependent on the fish life stage ( $s$ ), actual fish weight ( $W$ ), and sea water temperature;  $V_{sj}$  is the vulnerability of prey  $j$  to life stage  $s$ ;  $K_{sk}$  is the half-saturation constant for a fish in life stage  $s$  on zooplankton type  $k$ ; and  $Z_k$  is the concentration of zooplankton type  $k$  at the individual's location. These parameters differed between species, and also among life stages of the same species. The preference of sardine (anchovy) for smaller (larger) prey was introduced by prescribing decreasing  $V$  for larger zooplankton, thereby maximizing consumption rate in the presence of its favourite food composition. Fish length was calculated hourly from change in weight using length-weight and von Bertalanffy length-at-age relationships as:

$$\Delta L = \begin{cases} 0 & \text{if } \Delta W \leq 0 \\ \min(L_{t+\Delta t} - L_t, L^*) & \text{if } \Delta W > 0 \end{cases}; \quad L^* = (1 - e^{-k\Delta t}) \cdot (L_\infty - L_t)$$

where  $L_t$  and  $L_{t+\Delta t}$  are lengths from  $W_t$  and  $W_{t+\Delta t}$ , and  $k$ ,  $L_\infty$  are life-stage specific. A gain in weight implies an increase in fish length but length was not allowed to decrease, enabling the possibility for poor conditions to result in skinny fish.

Mortality of sardine and anchovy was due to three sources: natural mortality (decreasing with each lifestage), starvation, and predation. Natural and predation mortality act to reduce super-individuals' worth. Super-individuals reaching very small worths were removed from the simulation. Starvation mortality occurred when the fish weight dropped below certain percentage of the expected weight from its actual length (50% for larvae and 40% for juveniles and adults; based on Letcher et al. (1996) and Johnson and Evans (1991)) and resulted in the removal of the super-individual from the simulation by zeroing out its worth. Likewise, fish that reached a maximum permitted age (10 years) at the beginning of the year were also automatically removed (in practice the effective maximum age of the fish was ~8 years for sardine and ~5 years for anchovy, because older individuals represented less than 2% of the adult population). The super-individuals removed based

on age (always the same number) were then used to allocate to super-individuals to account for egg production the next year.

Eggs, yolk-sac-larvae and larvae were advected using ROMS horizontal velocities. Eggs and yolk-sac-larvae remained in the uppermost layer of the water column, while larvae were moved vertically to depths where they achieved maximum consumption rate. Juveniles and older individuals were moved (horizontally and vertically) following a kinesis approach (Humston et al., 2004; Watkins and Rose, 2013) using temperature and food availability as cues. With kinesis, individuals tend to move the same direction (and slow down) if local conditions are good (inertial component dominates), or swim randomly (random component dominates) when local conditions greatly deviated from optimal. The proximity to optimal conditions was represented differently for temperature and food availability. Temperature used a Gaussian-shape function with maximum value at a (prescribed) optimum temperature. The measure for food availability was given by the  $P$ -value

$$P\text{-value} = \frac{C}{C_m W}, \quad (3)$$

with the proportion of maximum consumption provided by food at that location. The function to determine proximity to optimal for food availability was the ascending portion of a Gaussian-shaped function that reached a maximum value of one (more food is always better). The kinesis algorithm was first applied in the horizontal direction, and then using the new horizontal location, kinesis was applied in the vertical dimension. Predatory individuals were moved according to a restricted-area search approach (Watkins and Rose, 2013), and their size and worth (abundance) were held constant throughout the simulation, as the only purpose for them was to impose spatially-varying and density-dependent mortality on the fish.

Reproduction of mature individuals occurred within a prescribed spawning season and within a range of temperatures. The timing of the batches' release depended on both the energy content of the individual (fitness; capital spawning) and its local growth rate (income spawning), and occurred whenever resting time conditions were satisfied. For further details of the IBM the reader is referred to R15.

### 3.3.2. Configuration for the CanCS

Starting from the standard configuration of R15, a number of model parameters were adjusted in order to fit the characteristics of the European sardine and anchovy. We first prescribed new values of the beginning and duration of the spawning season and the spawning temperatures (Coombs et al., 2006). We examined sea surface temperature (SST) images of recognized spawning and nursery grounds in order to estimate a typical temperature range of each species' habitat. Second, based on these new temperature preferences, we then adjusted the values of movement and bioenergetics that depended on specification of optimal temperature values. Finally, we substituted species- and life stage-specific values for growth-related and length-weight conversions. Those analyses resulted in the following set up: (a) sardine were allowed to spawn from November 1st to April 10th within 16.5–20.5 °C; (b) the spawning season for anchovy was April 10th to August 15th and was restricted to temperatures between 16.0 °C and 21.5 °C; (c) the optimal temperature for the juvenile and adult movement was the average value of these ranges: 18.5 °C for sardine and 19 °C for anchovy; (d) temperature coefficients for bioenergetics, particularly coefficients involved in the temperature effects on the maximum consumption rate, were modified according to these optima; and (e) growth and length-weights relationship parameters were also adjusted to match the characteristics of the European sardine and anchovy (see Table 1). As in R15, sardine and anchovy were represented by 10,000 super-individuals each, which turned out to be a suitable number to represent both populations based on sensitivity runs. Predatory fish were represented by 100 super-individuals with fixed worth over time.

Given the new parameter values, a number of preliminary runs were

performed to then calibrate the half saturation constants ( $K$ ) and natural mortality rates ( $M$ ).  $K$  values were calibrated for all life stages to yield realistic values of averaged weights-at-age and lengths-at-age. Then  $M$  was calibrated for eggs, yolk-sac larvae, and larvae in order to attain a stable long-term abundance (summed worth over super-individuals) for adult sardine and anchovy populations. This was possible by quasi-equilibrating fish recruitment rates and overall adult mortality. It should be noted that the average number of adults (and biomass) in the model depends strongly on the calibration of  $M$ , and hence must be seen as a prescribed outcome rather than a model result itself. Adjustments of the reproduction parameters were unnecessary, provided that the number of batches released by the fishes was satisfactory (see Section 6.2). No explicit migratory behaviour was incorporated in the kinesis algorithm for sardine and anchovy. However, in order to restrict anchovy individuals near the shelf, the direction of the random component of their velocity was biased shoreward when entering deep waters ( $z < -2000$  m; see R15 for details). All individuals were forced to remain within the model domain and outside the Bay of Biscay (north-eastern region of the domain), given that the stocks of this region are not the focus of the present study. Individuals of all three species were retained in the domain of interest by applying reflective boundary conditions, that is, by reversing their  $x$  or  $y$  velocities when individuals were about to leave the boundaries. Table 1 summarizes the model parameters that were adjusted and their final values for the CanCS. The rest of the parameter values were kept at the same values as reported in R15.

The IBM was initialized with an adult sardine biomass of 3.5 Mt (spread over super-individuals by age and assigned average weights at age), which is in the range of reported estimates (Barange et al., 2009). To the best of our knowledge, no consistent estimates of anchovy biomass have been reported in the CanCS; thus, a reasonable guess was made on the basis of the landings. The initial anchovy biomass in the simulation was set to 0.5 Mt. Super-individuals were randomly distributed from 14.5°N to 44.5°N, with sardines and anchovies around 150–250 km and 20–150 km offshore, respectively. Predatory super-individuals were initially randomly distributed across the whole domain.

All model output reported for sardine and anchovy are adjusted for the worth of each super-individual. Worth is treated like a statistical weight that determines how much super-individuals differentially contribute to the average or total or other processing of the output of individuals to get to the population-level. For example, adult abundance is the sum of all adult super-individuals' worth, average length-at-age is the average of the lengths of super-individuals using their worth as the statistical weightings in a weighted average. The details of the aggregation process used to go from super-individuals to population-level for most all of the outputs reported here is documented in Table of 6 of R15.

## 4. ROMS and NEMURO results

### 4.1. Sea surface temperature (SST)

The SST climatology simulated in the model (Fig. 3a–d) compares well with the climatology from the OSTIA database (Donlon et al., 2012; Fig. 3e–h). A feature with strong implications for both fish species is the variability of the Cape Blanc front, which is particularly well reproduced by the model. The front roughly coincides with the 26 °C isotherm and fluctuates between Cape Verde in winter (Fig. 3a and e) and Cape Blanc in summer (Fig. 3c and g). Upwelling is permanent between Cape Blanc and Cape Ghir, as suggested by the relative stable simulated and observed SST in the region, ranging between 17 and 21 °C year-round in both observations and the model.

The temporal dependence of the spatially-averaged SST is shown in Fig. 4. Seasonal and decadal-scale variability is apparent in both the observed signal and in the simulation. The correlation coefficient

**Table 1**

Bioenergetics and functional response parameters adjusted for sardine and anchovy in the CanCS.  $T_b$ : minimum temperature for spawning ( $^{\circ}\text{C}$ );  $T_T$ : maximum temperature for spawning ( $^{\circ}\text{C}$ );  $T_o$ : optimal temperature for movement ( $^{\circ}\text{C}$ ; Eq. 18 and Eq. 19 in R15);  $CQ$ ,  $TO$ ,  $TM$ ,  $TL$ : temperature effect on consumption ( $^{\circ}\text{C}$ ; eq. 8 in R15);  $V_{sj}$ : vulnerability of prey  $j$  to fish life stage  $s$  (Eq. 9 in RA15);  $K_{sj}$ : half saturation constant for fish stage  $s$  on prey  $j$  ( $\text{gm}^{-3}$ ; Eq. 9 in R15);  $M$ : natural mortality rate ( $\text{d}^{-1}$ );  $a$ ,  $b$ : length-weight relationship parameters ( $W = aL^b$ ;  $L$ : fish length in mm;  $W$ : fish weight in g). The rest of the parameter values are as in R15.

Symbol	Anchovy				Sardine			
	Egg/Ysac	Larva	Juvenile	Adult	Egg/Ysac	Larva	Juvenile	Adult
$T_b$	–/–	–	–	16.5	–/–	–	–	16.75
$T_T$	–/–	–	–	21.5	–/–	–	–	20.25
$T_o$	–/–	–	19.0	19.0	–/–	–	18.5	18.5
$CQ$	–/–	10.0	10.0	10.0	–/–	13.5	13.0	13.0
$TO$	–/–	19.0	20.0	20.0	–/–	18.0	17.5	17.5
$TM$	–/–	23.0	23.5	23.5	–/–	21.0	21.0	21.0
$TL$	–/–	30.5	29.0	29.0	–/–	29.0	31.0	31.0
$V_{sj}$	–/–	1.0, 0.5, 0.0	0.2, 1.0, 0.2	0.2, 0.4, 1.0	–/–	1.0, 0.1, 0.0	1.0, 0.2, 0.2	1.0, 0.4, 0.2
$K_{sj}$	–/–	0.04, 0.04, –	0.09, 0.09, 0.09	0.09, 0.09, 0.09	–/–	0.1, 0.1, –	0.05, 0.05, 0.05	0.07, 0.07, 0.07
$M$	0.198/0.137	0.106	0.009	0.002	0.753/0.482	0.147	0.011	0.001
$a$		$3.0 \times 10^{-7}$	$1.0 \times 10^{-5}$	$7.0 \times 10^{-6}$		$5.4 \times 10^{-6}$	$5.4 \times 10^{-6}$	$5.4 \times 10^{-6}$
$b$		3.9	2.9	3.0		3.1	3.1	3.1

between modelled and observed time series is  $r = 0.99$  for the monthly series (thin lines) and  $r = 0.92$  for the low frequency curves (thick lines). This latter value is particularly important as the focus of the present paper is on the control of environmental conditions in driving decadal-scale variability of the sardine and anchovy populations. Likewise, the linear trend of the two SST series during the overlapping period is of the same order:  $0.017 \pm 0.006 \text{ }^{\circ}\text{C}/\text{year}$  in the model and  $0.026 \pm 0.005 \text{ }^{\circ}\text{C}/\text{year}$  in the observations. However, the model overestimates the maximum monthly SST by about  $0.5 \text{ }^{\circ}\text{C}$ . Such deviation is primarily due to SST biases in some upwelling regions, particularly off Iberia (Fig. S1). Off NW Africa, the biases are smaller with the exception of some areas off Cape Ghir and Cape Blanc. We attribute these biases to the coarse atmospheric forcing, particularly winds,

which likely results in an underestimation of the wind stress curl in some locations along the coast and therefore also underestimated Ekman pumping. Correlations between the low-frequency SST series typically lie above  $r = 0.8$  across the domain. The lowest correlations are found in the Gulf of Cadiz and south of Cape Blanc, but they are still in a reasonable range ( $r \approx 0.4\text{--}0.6$ ). Modelled near-surface velocities display a seasonality that is coherent with the SST, and match overall velocity patterns derived from drifters (Fig. S2).

4.2. Surface chlorophyll

The position of the surface chlorophyll (*chl*) maximum oscillates latitudinally and is closely related to the band of maximum upwelling

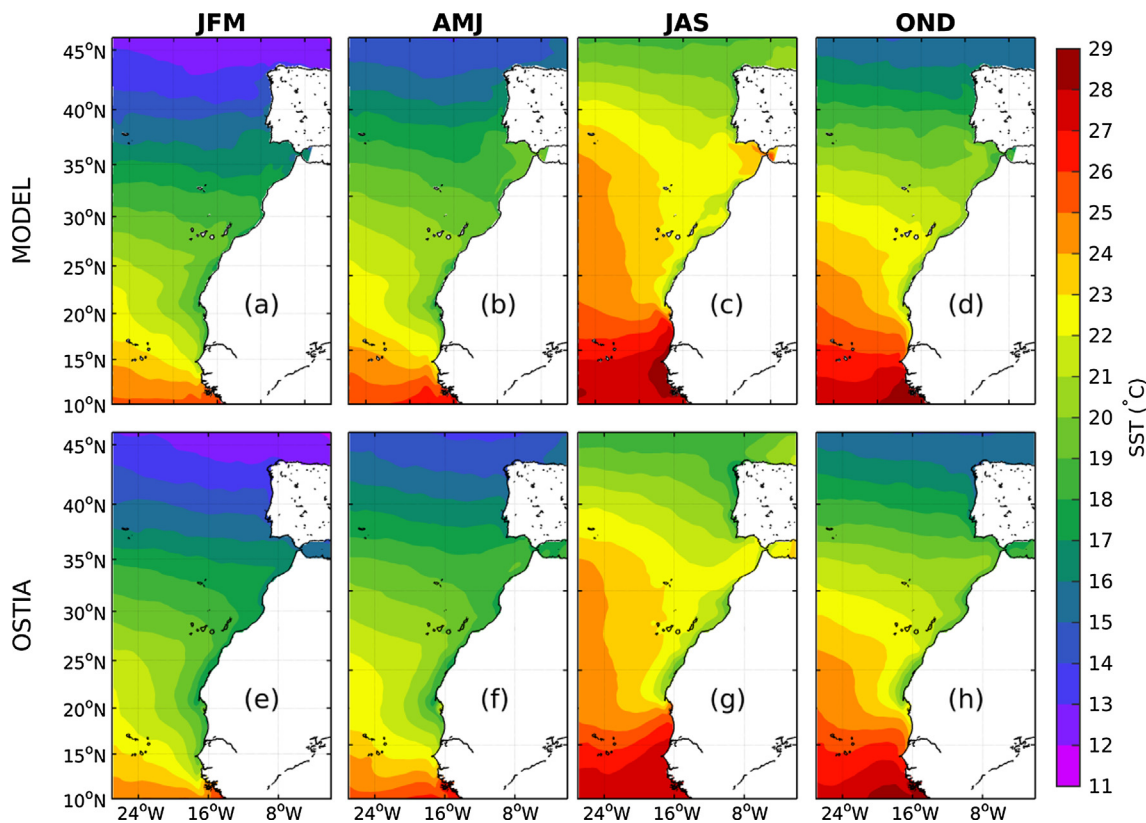


**Fig. 3.** Simulated (a–d) and observed (e–h) seasonal SST climatology. In both cases the climatology corresponds to the period 1985–2007, the period in which satellite SST data are available. Observations consist of monthly OSTIA products at  $1/4^{\circ}$  resolution (Donlon et al., 2012).

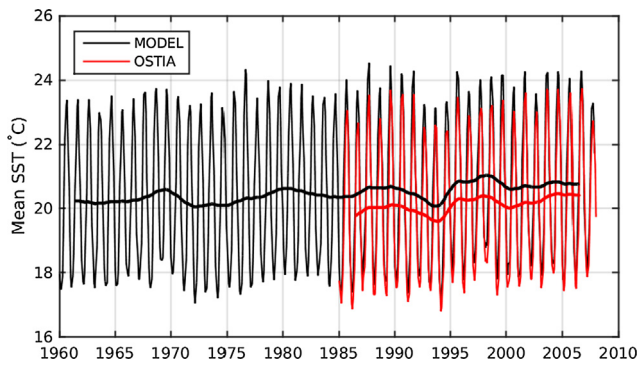


**Fig. 4.** Simulated and observed (OSTIA product) SST over the CanCS. The time series corresponds to spatial averaged SST values over the domain shown in Fig. 3. Monthly (thin lines) and low-frequency (thick lines) series are shown. The low-frequency series was derived by applying a Gaussian low-pass filter with 1/18 month<sup>-1</sup> cut-off frequency.

intensity suggested by the SST and the surface velocity climatology (Fig. 5a–d). The maximum moves from the coast of Mauritania-Senegal in winter (Fig. 5a) to the north of Cape Blanc in summer (Fig. 5c). The overall *chl* maximum off NW Africa occurs during the spring, as coastal *chl* increases from Cape Verde to Cape Bojador ( $chl > 7 \text{ mg m}^{-3}$ ; Fig. 5b). Throughout the rest of the year, such high *chl* values are only found in the vicinity of Cape Blanc during the summer (Fig. 5c). In the open ocean, the model reproduces a seasonal modulation of *chl* associated with oscillations of the North Atlantic Subtropical Gyre: *chl* diminishes towards the summer as the gyre approaches the CanCS domain, and the opposite pattern occurs in winter. Traces of the North Atlantic spring bloom are also apparent in the simulation northwest of the Iberian Peninsula around 45°N, where *chl* increases substantially from winter to spring. All these patterns are present in the SeaWiFS *chl* climatology (SeaWiFS, 2003) shown in Fig. 5e–h, although with some

quantitative differences. For example, compared to SeaWiFS values, the model underestimates coastal *chl* off NW Africa during winter and fall, and overestimates *chl* in the open ocean during spring.

### 4.3. Zooplankton

Surface zooplankton follows the overall *chl* spatial pattern (Fig. 6) and the distribution of the three zooplankton types in the model is consistent with their unequal preferences for PS and PL as prey. Larger zooplankton (ZP) dominates onshore as they preferably feed on PL, which is well adapted to nutrient-rich waters and thrives in the coastal upwelling region (not shown). The opposite applies to the smaller zooplankton (ZL and ZS) whose distributions are more evenly spread among onshore and the more nutrient-poor offshore waters. ZP is greatly restricted to the coast (Fig. 6c), as it mainly feeds on PL and ZL. Total zooplankton is most abundant between Cape Verde and Cape Bojador. Further north, two spots of high zooplankton concentration are distinguished along the coast over 28°N and 33°N (Fig. 6b and c), which match the locations of the two northern sardine stocks reported for NW Africa. Both phytoplankton and zooplankton varied throughout the simulation at seasonal (maximum and minimum surface values by early spring and early fall respectively) and decadal time scales (Fig. 7).

## 5. Results of the IBM

### 5.1. Sardine and anchovy spatial distributions

The seasonal climatology of sardine biomass density is shown in Fig. 8. Sardine eggs occur mainly off NW Africa during winter (Fig. 8a) and they also appear widespread during fall (Fig. 8d), including off Iberia where temperature is warm enough for spawning towards the end of the year. Larval abundances peak in winter and are most abundant off Cape Blanc (Fig. 8e) where, according to the zooplankton distribution shown in Fig. 6a, the feeding conditions are particularly

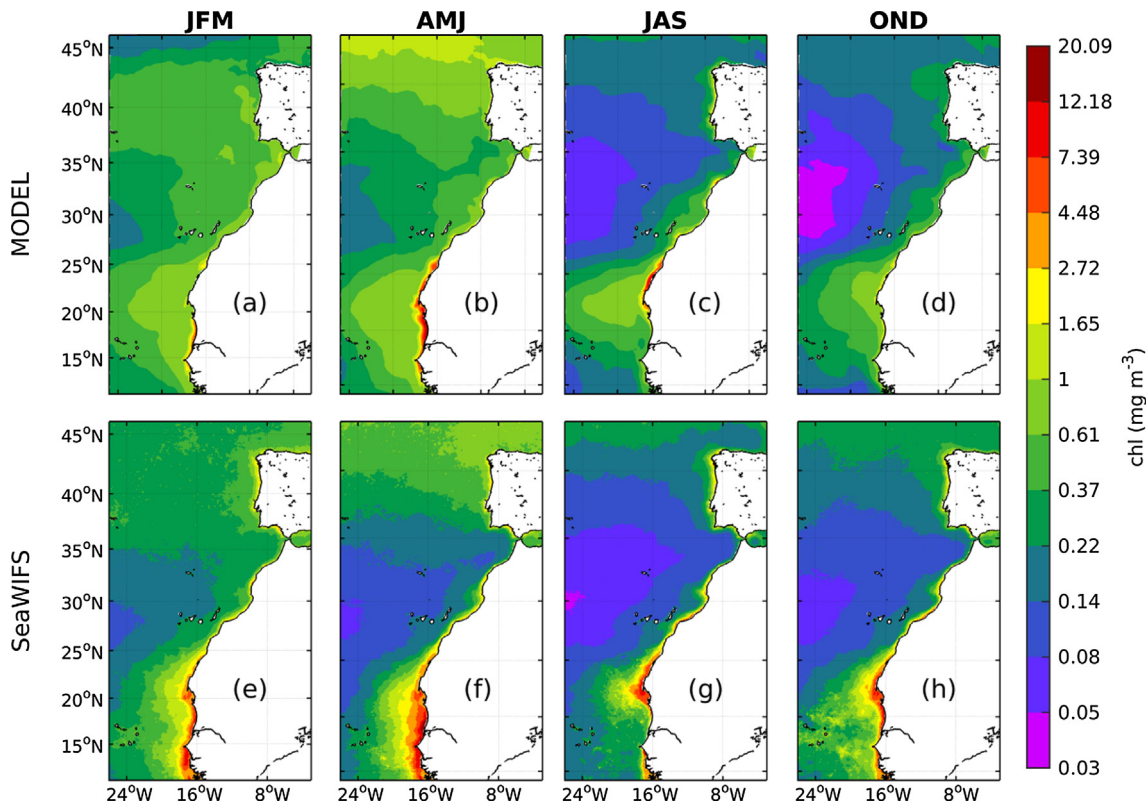


**Fig. 5.** Simulated (a–d) and SeaWiFS (e–h) seasonal *chl* climatology. In both cases the climatology corresponds to the period 1997–2007.

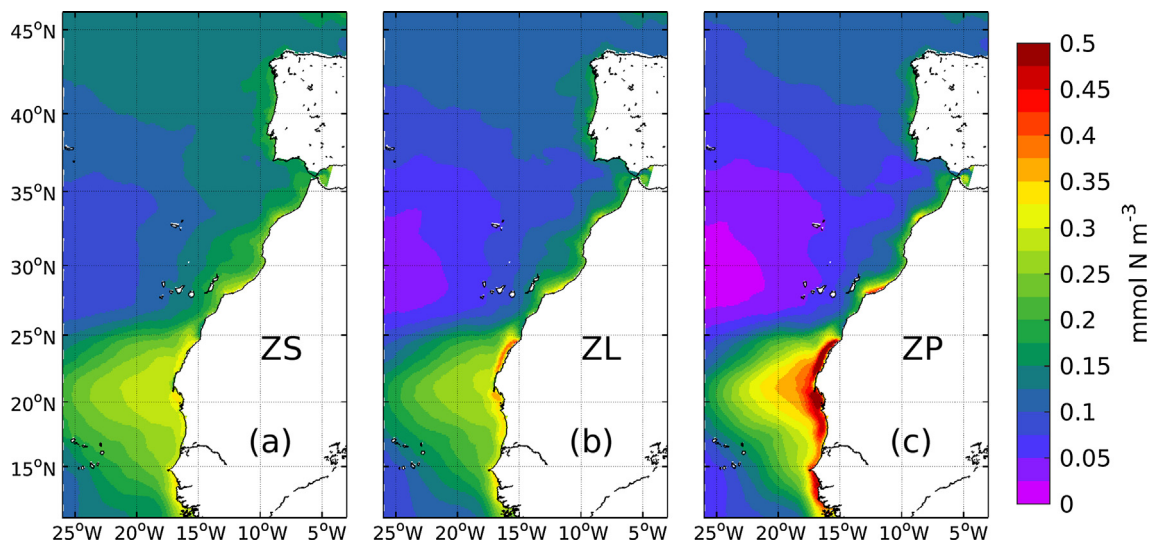


Fig. 6. Mean surface zooplankton obtained in the historical simulation: (a) small zooplankton ZS, (b) large zooplankton ZL, and (c) predatory zooplankton ZP.

favourable. Juvenile biomass peaks some months later during spring and summer (Fig. 8j and k). The adult population is largely restricted to the coastal area between Cape Blanc and the Strait of Gibraltar (Fig. 8m–p).

Meridional shifts of adult sardines are seasonal. During winter and spring, adults move southwards to the vicinity of Cape Verde (Fig. 8m and n) driven by both food availability and favourable temperatures in the region (approximately 18 °C, Fig. 3a and b). During summer and fall, when upwelling conditions are more favourable farther north, sardines move from the lower latitudes and become most abundant from Cape Blanc to the Strait of Gibraltar (Fig. 8o and p). Aggregations and dispersal of the sardine population is also captured by the model. During fall, sardines appear split into three groups with boundaries roughly situated in Cape Ghir and Cape Bojador (Fig. 8p). This configuration becomes less obvious from winter to spring as the central and northern groups partially merge (Fig. 8m and n), and fades out during summer (Fig. 8o). Altogether, the sardine biomass spatial pattern and its seasonality, particularly the transition from a three-stock distribution to a homogeneous population in summer, qualitatively agrees with estimates from acoustic surveys (Aristegui et al., 2009).

The seasonal spatial distribution of anchovy is different from that of sardine (Fig. 9). Adult anchovy gather onshore in the northern part of Morocco and, to a lesser extent, in the Gulf of Cadiz (Fig. 9m–p). Eggs peak during spring (Fig. 9b), larvae peak during spring and summer (Fig. 9f and g), and juveniles reach their maximum during fall (Fig. 9l). Anchovy do not vary in their horizontal distributions as much as sardine, and become noticeably scarce in the nutrient-rich waters between

Cape Bojador and Cape Blanc. An explanation of this result is given in Section 6.3.

The latitudinal position of adult sardine and anchovy distributions moderately change throughout the simulation. The centre of mass of the sardine population (age-1 and older individuals;  $YS_{cm}$ ) lies within 26.2°N and 28.8°N and fluctuates at several time scales (Fig. S3); the most apparent scale being the seasonal signal described above.  $YS_{cm}$  is at a minimum by mid-April and a maximum by late November. Decadal-scale variability is also evident in  $YS_{cm}$ . Major changes at these scales consist of a southward shift of the sardine during the first half of the 1970's and a northward displacement by the late 1990's. The centre of mass of anchovy (orange line;  $YA_{cm}$ ) resides about 7° north of that calculated for sardine, and displays a weaker seasonal signal. Decadal-scale variability is also apparent in  $YA_{cm}$  and is likewise weaker than the signal for sardine. Both  $YS_{cm}$  and  $YA_{cm}$  show a positive trend during the simulation (0.048°/year and 0.028°/year, respectively), presumably driven by the warming of sea water temperatures (Fig. 4).

### 5.2. Fish length, weight, diet and predation

Fish weights-at-age and lengths-at-age relations remained fairly constant throughout the simulation and were in the range of observed values (Fig. 10). Mean decadal weights-at-age differed from each other by less than 10 g for sardines (Fig. 10a) and by around 3 g for anchovies (Fig. 10b). Sardine age-1 represented 31% of the sub-adult and adult (age-1 and older) population on January 1 of each year (in average). For anchovy, this percentage was 51%. Average number of batches per

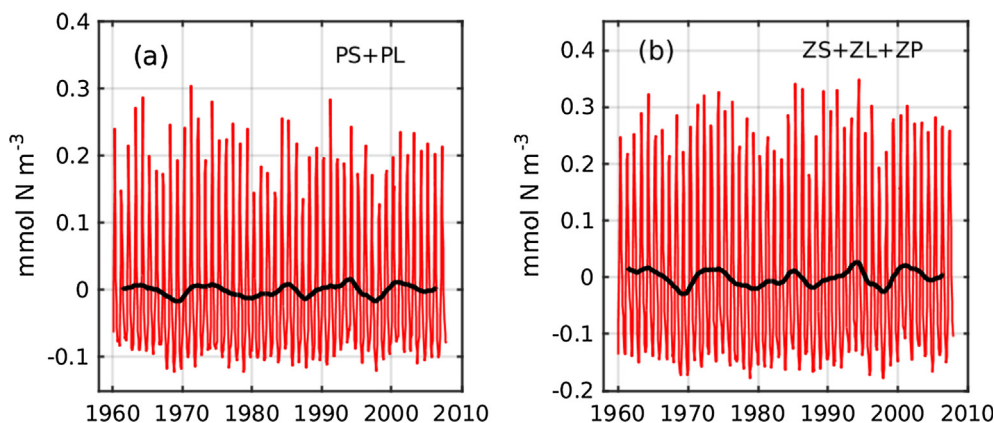


Fig. 7. (a) Simulated surface phytoplankton anomaly in the CanCS. Values are the sum of small and large phytoplankton concentration (PS + PL) spatial average. Anomaly refers to deviation with respect the 1960–2007 mean. Both seasonal (red line; monthly data) and decadal-scale variability (black thick line; low-pass filtered series) can be distinguished in the series. (b) Same as (a) for surface zooplankton (ZS + ZL + ZP). (For interpretation of the references to colour in this figure legend, the reader is referred to the web version of this article.)

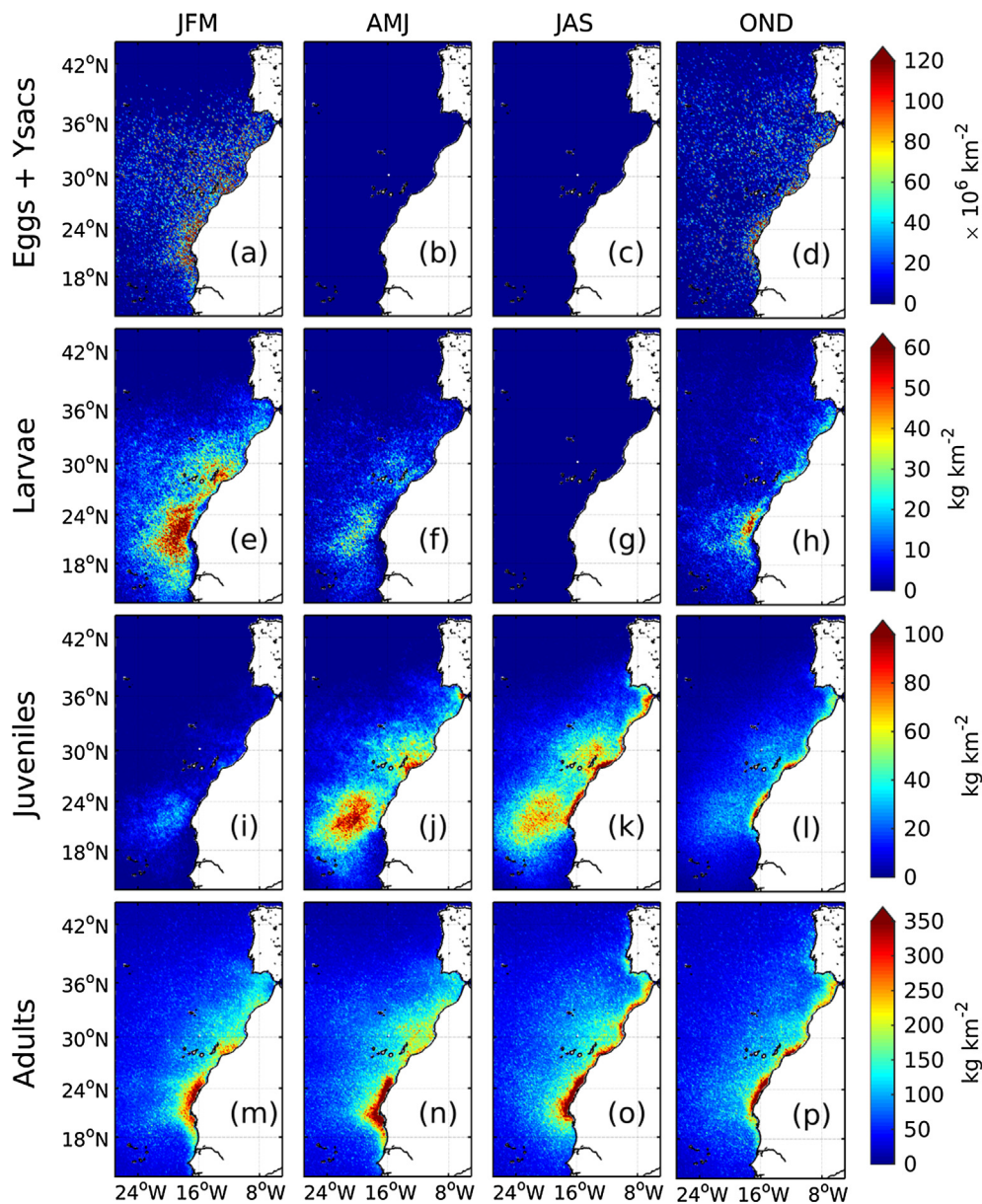


Fig. 8. Simulated seasonal climatology of sardine abundance and biomass. Abundance of eggs and yolk-sac larvae is given in million individuals per km<sup>2</sup> (a–d). Biomass of larvae (e–h) and subsequent life stages (juveniles, i–j; age-1 and older individuals, m–p) is given in kg·km<sup>-2</sup>.

adult individual and spawning season was 7–8 for sardine and 13–14 for anchovy. Sardine and anchovy produced a yearly number of eggs of  $(9.0 \pm 0.9) \times 10^{15}$  (avg  $\pm$  sd) and  $(4.0 \pm 0.7) \times 10^{15}$  respectively, and the largest fractions of the total egg production came from age-2 (27% sardine, 46% anchovy) and age-3 (22% sardine, 23% anchovy) individuals.

Adult sardines experienced averaged ambient temperatures of  $20.9 \pm 1.4$  °C, whereas anchovies were found in slightly colder waters ( $18.4 \pm 1.6$  °C). This implies a mean deviation of about 2 °C and 1 °C warmer than the prescribed temperature optimum used for movement. The greater temperature deviation for sardines is likely because sardine was not forced to swim towards nearshore (i.e., colder) waters to find enough of its preferred food (ZS). The preference of sardines to graze on ZS is reflected in their mean diet composition calculated from realized consumption (Eq. (3)). Adult sardines gained most of their energy from ZS (70% of their diet), while ZL and ZP represented 21% and 9% of total energy ingestion. Anchovy diet composition was more varied and opposite to that of sardine being dominated by ZP (57% ZP, 27% ZL and 16% ZS). Predation mortality took place where sardines were most

abundant, which occurred in three areas bounded by Cape Bojador and Cape Ghir (Fig. S4). These locations match the general locations of the assumed stocks off NW Africa. Predation on anchovy occurred mainly in the northern and central regions.

### 5.3. Biomass and abundance variability

The time series of adult biomasses is shown in Fig. 11a. Simulated sardine biomass averaged  $4.0 \pm 0.4$  Mt, within the range of reported estimates, whereas anchovy biomass was about 4–5 times smaller and averaged  $0.9 \pm 0.2$  Mt (note the different vertical scales in the Fig. 11a). Both species exhibited interannual and decadal-scale variability in the historical simulation. The historical maximum of sardine biomass was 4.9 Mt and was attained by the mid 1970’s. This maximum was followed by a long decrease until the sardines’ historical minimum in 1990 at 3.7 Mt. Subsequently, sardine recovered during the first half of the 1990’s, reaching 4.5 Mt in 1995, and then declined again during the second half of that decade to 3.4 Mt in 1999. Throughout the rest of the simulation, sardine recovered again slightly. Anchovy biomass

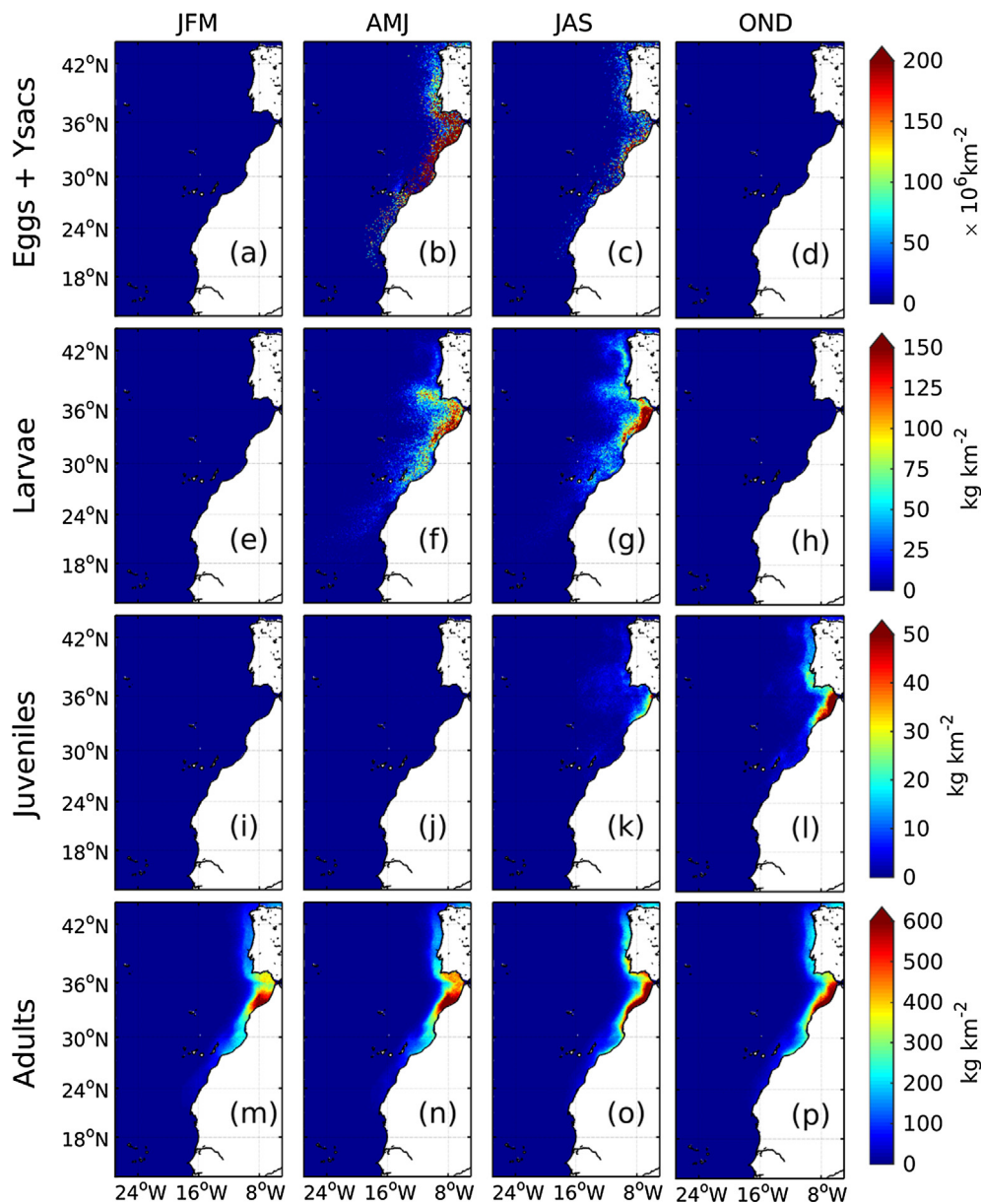


Fig. 9. Simulated seasonal climatology of anchovy abundance and biomass. Abundance of eggs and yolk-sac larvae is given in million individuals per  $\text{km}^2$  (a–d). Biomass of larvae (e–h) and subsequent life stages (juveniles, i–j; age-1 and older individuals, m–p) is given in  $\text{kg}\cdot\text{km}^{-2}$ .

fluctuated nearly in-phase with that of sardines (correlation coefficient  $r = 0.58$ ), which is consistent with the synchronous variability observed in landing records (Fig. 1). Adult abundance (Fig. 11b; total number of individuals) varied similarly to biomass except for isolated periods during which a prominent increase in biomass (due to a gain in weight of individuals) was not similarly apparent in abundance (e.g., sardine during the mid-1990’s).

A direct comparison of the simulated biomass and catches of sardine and anchovy in NW Africa (anomalies; Fig. 11c and d), the latter used as a proxy of the actual biomass, highlights qualitative similarities and some discrepancies between simulated values and observations. The model does well in two aspects; first the time scale and amplitude of the variability are similar for both species. Second, and most importantly, sardine and anchovy vary synchronously. Major discrepancies are shifts in the simulated series with respect to the catches during certain periods (mainly 1985–1998). The specific reason for this disagreement is unclear but, bearing in mind the simplifications and uncertainties associated with the model, as well as the limitations of landings as a proxy for biomass, a mismatch is not unexpected. Factors not explicitly

represented in the model, such as fishing mortality, could partially explain the disagreement.

## 6. Analysis of sardine and anchovy dynamics

### 6.1. Biological processes

The biological processes responsible for sardine and anchovy population variability are investigated in this section. Since adult mortality rates were relatively constant, the major biological processes that would cause interannual variation are adult growth affecting fecundity and growth or development rates affecting survival of young-of-the-year life stages. Predatory fish exerted dynamical and potentially density-dependent mortality on adult anchovy and sardine, but the magnitude of the mortality was small compared to the constant natural mortality rates. Therefore, we focused on number of eggs spawned per individual and age-0 survival rates during the prior year. These two factors determine recruitment, and therefore also the subsequent year’s size of the adult population. We discern below the relative contribution

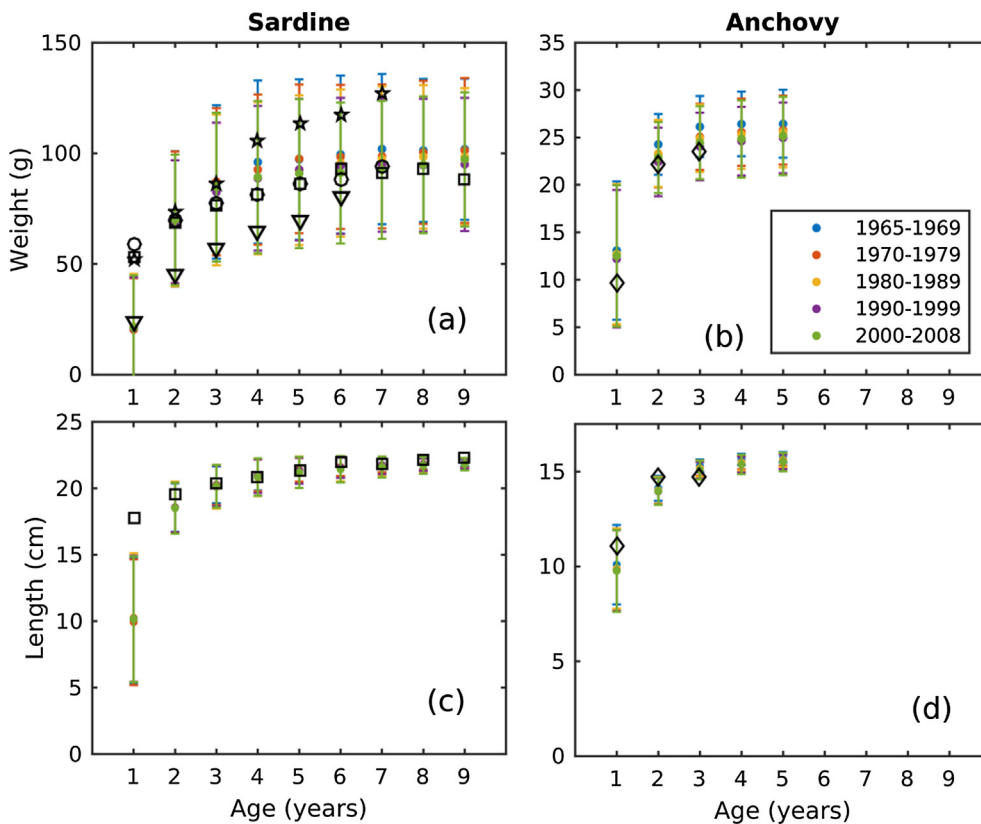


Fig. 10. Fish weights-at-age and lengths-at-age. Dots in colour correspond to mean modelled decadal values. Error bars represent one standard deviation below and above the mean (error bar lengths are two times the standard deviation). Anchovy individuals older than 5 years of age were at very low numbers so are not shown. Black markers are averaged weights- and lengths-at-age in catches reported for different periods and areas: 2014–2016 in western Iberia (squares; ICES, 2014, 2015, 2016a); 1987–2015 in the Gulf of Cadiz (diamonds; ICES, 2014); 1990–2016 western Iberia (inverted triangles; ICES, 2016a); 1983–1990 South of Cape Bojador (circles; FAO, 2001); 1990–2002 South of Cape Bojador (stars; FAO, 2012). (For interpretation of the references to colour in this figure legend, the reader is referred to the web version of this article.)

of these two factors in determining the interannual variation in sardine and anchovy adult biomass.

Our analysis is based on examining conditions during anomalously good and bad years. Good versus bad years were measured in terms of the relative increase of the adult population on January 1 from that year to the next,  $\Delta p_y = (na_{y+1} - na_y)/na_y$ . Here,  $na_y$  denotes the number of adults on January 1 of year “y”. We used the relative change because it controls for the differences in adult abundances through the simulation; absolute changes depend on the number of adult present because more adults give rise to more individuals the following year. Anomalously good and bad years – hereafter simply referred to as good and bad years – were then defined as those years in which the relative increase/decrease of the population lied outside the range of one standard deviation of the historical time series ( $\pm 1$  SD in Fig. 12). Since sardine and anchovy in the CanCS tend to fluctuate synchronously, some anomalous years are coincident for the two species (e.g., 1969, 1974, 1983 and 1989). Also, a single year being good for one species and bad for the other was not found in the historical series.

Age-0 (egg to juveniles becoming age-1 on January 1) survival rate and yearly production of eggs (Fig. S5) were compared between good and bad years. Egg production was examined as the number of eggs per adult individual (eggs/ind) to account for changes in adult spawners, and to link egg production to growth rate differences. Individual spawners in good body condition (i.e., larger body weights for their age), produce more eggs than smaller individuals. We focused on age-2 and age-3 individuals because these ages account for the majority of the total egg production.

The eggs/ind anomalies for good and bad years are shown in Fig. 13. Positive and negative anomalies generally coincide with good and bad years for sardine (red bars had high anomalies), while eggs/ind anomalies for anchovy did not appear to be related to good versus bad years. For instance, age-2 eggs/ind were less than normal (i.e., outside of a SD) in 6 out of a total of 9 good years identified for anchovy, which suggests that interannual variation in egg production does not greatly influence recruitment. In contrast, age-0 survival is relevant to both

species because survival rate was generally above (below) its average value during good (bad) years for both sardine and anchovy (Fig. 14; upper row). This interpretation is supported quantitatively by the correlations between eggs/ind, age-0 survival and  $\Delta p$  over the whole set of anomalous years (good plus bad years; Table 2): eggs/ind and  $\Delta p$  correlates highly ( $r > 0.7$ ) only for sardine, whereas the correlation between age-0 survival and  $\Delta p$  is high for both sardine ( $r = 0.84$ ) and anchovy ( $r = 0.93$ ). Hence, the conclusion that can be drawn from Fig. 13, Fig. 14 and Table 2, is that major changes in recruitment are associated with both changes of age-0 survival and egg production for sardine, and primarily with age-0 survival for anchovy.

### 6.2. Role of temperature and food

To determine which environmental condition primarily controls the variability of age-0 survival, we further analysed survival rates of feeding (larva to juvenile becoming age-1 on January 1) and non-feeding (egg to yolk-sac becoming larva) early life stages (Fig. S5). Fig. 14 (middle and bottom panels) shows that, for both sardine and anchovy, survival anomalies of the feeding stages is positive (negative) during good (bad) years, while there is no general agreement between survival and good versus bad years for the non-feeding stages. In fact, survival of feeding stages correlated highly with  $\Delta p$  for sardine ( $r = 0.86$ ) and anchovy ( $r = 0.95$ ), whereas the same correlation for non-feeding stages were even negative (although low; Table 2). This indicates that survival of feeding stages, and hence probably food availability (and perhaps temperature to a lesser extent), is key for both species (see also Section 6.4). This is particularly true for sardine because good and bad years for this species coincide also with years of high and low egg production (per individual), and egg production depends on the actual fish weight and availability of food.

### 6.3. Origin of the synchronous variation

The common reliance on food emerges as the likely origin for the

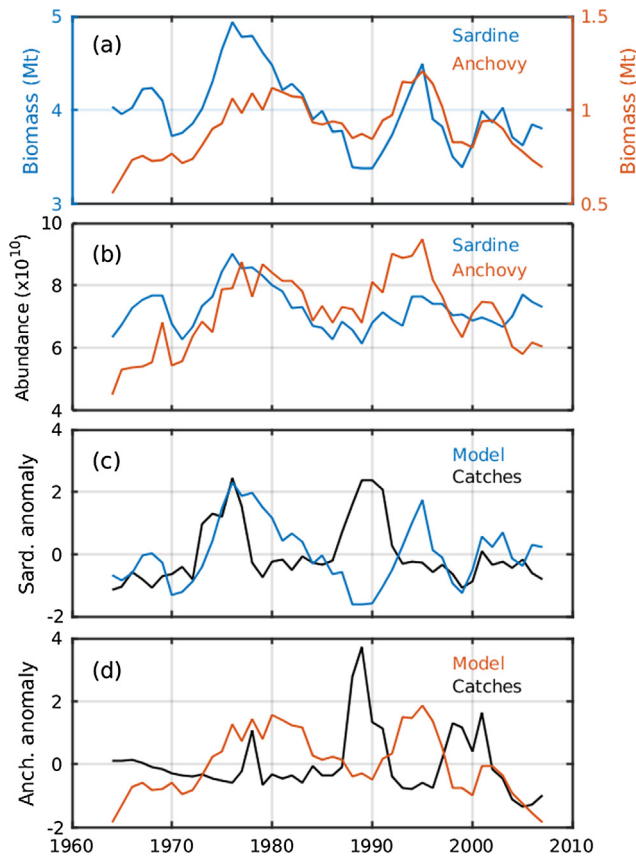


**Fig. 11.** Simulated historical series of sardine and anchovy biomass (a) and abundance (b). Values are for age-1 and older individuals on January 1st of each year. (c) Model sardine biomass and annual catches anomaly in NW Africa. Anomaly was computed as  $(y - \bar{y}) / \sigma_y$ , where “y” denotes the original time series,  $\bar{y}$  its regression line and  $\sigma_y$  its standard deviation. (d) Same as (c) for anchovy.

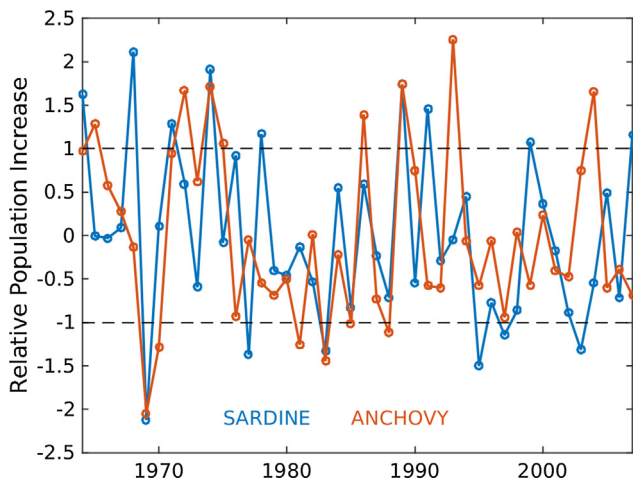


**Fig. 12.** Yearly relative increase of sardine and anchovy adult populations (standardized) in the historical simulation. The population increase in a given year “y” was computed as  $\Delta p_y = (na_{y+1} - na_y) / na_y$ , where  $na_y$  and  $na_{y+1}$  denote the number of adults on January 1st of years “y” and “(y + 1)”. Years with  $\Delta p$  lying above and below one standard deviation from the mean (dots outside dashed lines) are respectively defined as good and bad years for the fish.

synchronous variation of sardine and anchovy in the historical simulation. This interpretation relies on the fact that, independent of their different phenology, sardine and anchovy populations experience similar changes of feeding conditions from year to year. Since sardine and anchovy settle in different locations, synchrony is possible

whenever the response of zooplankton to climatological forcing occurs at a sufficiently large spatial scale to be felt similarly in the main sardine and anchovy habitats. To investigate this possibility, we conducted an empirical orthogonal function (EOF) analysis of simulated surface zooplankton, which permitted the identification of the main spatial patterns of variability generated by the model. Because our interest is in variability at interannual time scales, the EOF analysis was applied to yearly time series. The EOF modes described next correspond to total zooplankton (ZS + ZL + ZP), but similar patterns of variability were identified based on EOFs calculated for each individual zooplankton type (not shown).

The first mode (EOF #1; Fig. 15a) captures domain-wide changes in zooplankton along the boundary current that equally affect the main habitats of anchovy (coastal northern NW Africa; Fig. 9) and sardine (offshore central-southern NW Africa; Fig. 8). Furthermore, EOF #1 accounts for 39% of the total zooplankton variance, indicating that to a first approximation both sardine and anchovy experience similar interannual variability of food abundance – the associated principal component (or temporal coefficient) varies at a typical time scale of 7–10 years (Fig. 15g). Likewise, EOF #3 (14% of variance; Fig. 15c) is homogeneous across a broad region offshore Morocco-Sahara where the bulk of sardine and anchovy populations reside (however, a fraction of sardine early life stages is found south of Cape Blanc; Fig. 8), and consequently also leads to roughly similar changes in feeding conditions for the two species. In contrast, EOF #2 reverses sign in the vicinity of Cape Bojador (Fig. 15b), thereby implying opposite feeding conditions for sardine and anchovy (Figs. 8 and 9). However, the second mode accounts for 16% of the total variance, which is less than half the variance explained by EOF #1 (39%) and roughly a third of the contribution of the first and third modes combined (53%). Altogether, the EOFs show that sardine and anchovy were exposed to similar feeding conditions in the simulation, whereby years of high (low) food abundance for one species were also of high (low) abundance for the other).

Next, we analyse the interannual variability of ocean temperature and its likely impact on the fish populations. Although temperature emerges as a secondary environmental variable when compared to food (survival of non-feeding age-0 does not control the variability of recruitment), temperature is expected to play a role on the fish population dynamics by modulating survival of feeding age-0 and fecundity through bioenergetics (i.e., consumption and respiration). Hence, we further examine whether temperature varies simultaneously over sardine and anchovy habitats and thereby acts as an additional driver (along with food) for the synchronization of the two species. The EOFs for surface temperature (Fig. 15d–f) are coherent over even larger spatial scales than those for zooplankton, and confirm the synchronous effect of large-scale variation in temperature on both anchovy and sardine.

#### 6.4. Response to upwelling

The previous section reveals that sardine and anchovy primarily respond to domain-wide environmental forcing. However, there are differences between sardine and anchovy that suggest that localized factors may also differentially affect the two species. Sardine recruitment depends on food availability in two ways (via both age-0 survival and spawning), and anchovy and sardine showed different spatial distributions (Figs. 8 and 9). On the other hand, wind affects productivity in upwelling systems and often has an important effect on sardine and anchovy dynamics (Cury and Roy, 1989). The response of these two species to wind-driven upwelling is investigated next.

Fig. 16 shows the historical mean surface wind stress (left panel) along with associated anomalies averaged for good and bad years for each species. Intensification of the mean wind pattern implies enhanced upwelling and abundance of food; thus it is not surprising that good (bad) years are essentially characterized by anomalously strong (weak)

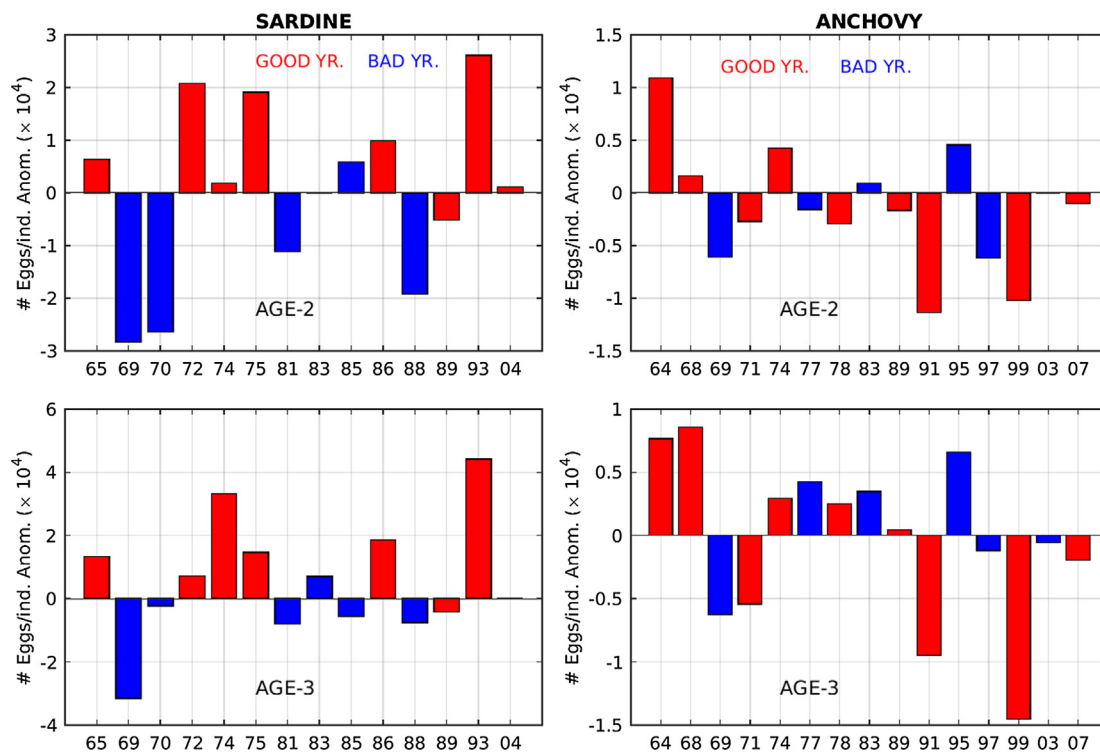


**Fig. 13.** Number of eggs per individual anomaly during good and bad years for sardine (left) and anchovy (right) in the historical simulation. For a particular age class, eggs/ind refers to the yearly production of eggs by the age class in question divided by the number of individuals of the age class on January 1st that year. Only values for age-2 and age-3 individuals are shown. Anomalies for good and bad years are represented with red and blue colour bars respectively, and refer to deviation from the 1964–2007 mean. (For interpretation of the references to colour in this figure legend, the reader is referred to the web version of this article.)

northeasterly winds. The weakening of upwelling-favourable winds during bad years is particularly pronounced and generalized across the domain, which indicates that the more dramatic the wind drop, the poorer the conditions for sardine and anchovy.

While the difference in wind stress between the mean and bad years for both sardine and anchovy was very evident, the difference between mean and good years was less noticeable (Fig. 16). The panels corresponding to good years (Fig. 16b and d) do not display an overwhelming enhancement of the mean wind pattern, especially for anchovy. Sardines benefit (good versus mean years) from strong northeasterly winds in the open ocean and over coastal areas off Iberia, Mauritania, and Senegal; but sardine only benefit from a moderate wind increase where they are most abundant (i.e., between Cape Blanc and the Strait of Gibraltar) (Fig. 8m–p). The optimal environmental window hypothesis (Cury and Roy, 1989) offers an explanation: recruitment success increases with upwelling intensity and food supply up to certain wind speed threshold, but decreases as stronger winds enhance advection of larvae. Increased advection of larvae would lead to higher overall mortality of age-0 individuals, which is one of biological processes identified from modelling results here as a determinant of changes in adult population abundance. In this case, stronger advection is consistent with an anomalously high export of larvae from Morocco-Sahara to Mauritania-Senegal, where food is not scarce (Fig. 6) but ambient temperatures are too warm (Fig. 3) for larvae and juveniles.

Anchovy are more sensitive to the wind regime than sardines because annual changes in population abundance for anchovy was almost entirely dependent on age-0 survival, while sardine changes were also influenced by adult growth and fecundity. Anchovy benefit from enhanced upwelling off Iberia and Sahara as well as from weak winds in the northern part of Morocco, around Cape Ghir (Fig. 16). This region roughly coincides with the southern boundary of the main anchovy habitat generated in the simulation (Fig. 9m–p). Enhanced upwelling (stronger winds) along the Iberian coast provides nutrient supplies from the north, while weaker than normal northeasterly winds around Cape

Ghir prevent southward advection of larvae. One caveat to this interpretation is that anchovy settle farther north than sardine and therefore farther away from the unfavourable (warm) region off Mauritania-Senegal; however, anchovy larvae require weaker southward winds to remain closer to the more northern region.

The explanation for this apparent contradiction is that ambient conditions off central Morocco are not favourable for anchovy larvae. This is indeed reflected by the mean conditions of food (*P*-value) and temperature (effect on consumption) experienced by anchovy larvae in the simulation (Fig. 17). While temperatures are near optimum from Cape Ghir to Cape Blanc, food is only abundant along a narrow coastal strip between these two capes. Therefore, considering that a large fraction of larvae is driven offshore (Ekman drift) as they are transported southward, advection would not increase the chances of larval survival; but rather the opposite. In fact, aside from the nutrient-rich waters of Mauritania-Senegal, the most suitable locations for anchovy larvae in term of food are the northern part of Morocco and the waters off Iberia, where upwelling conditions are most favourable during the anchovy spawning season (spring to summer). The spatial distribution of the preferred food for anchovy larvae during the spawning season (*P*-value in Fig. 17), further explains why a single and stable anchovy population south of its settlement location in the model (northern Morocco) would not be feasible: recruitment in such situation would be greatly constrained by larval mortality.

## 7. Summary and discussions

We implemented an end-to-end model of sardine and anchovy originally developed for the California Current to sardine and anchovy in the CanCS. The new version of the model was used to simulate 1958–2007 and reproduces decadal-scale variability of sardine and anchovy population abundance and biomass. Basic biological traits prescribed for these two species lead to similar and synchronous biomass variability of sardine and anchovy, a distinctive feature of the

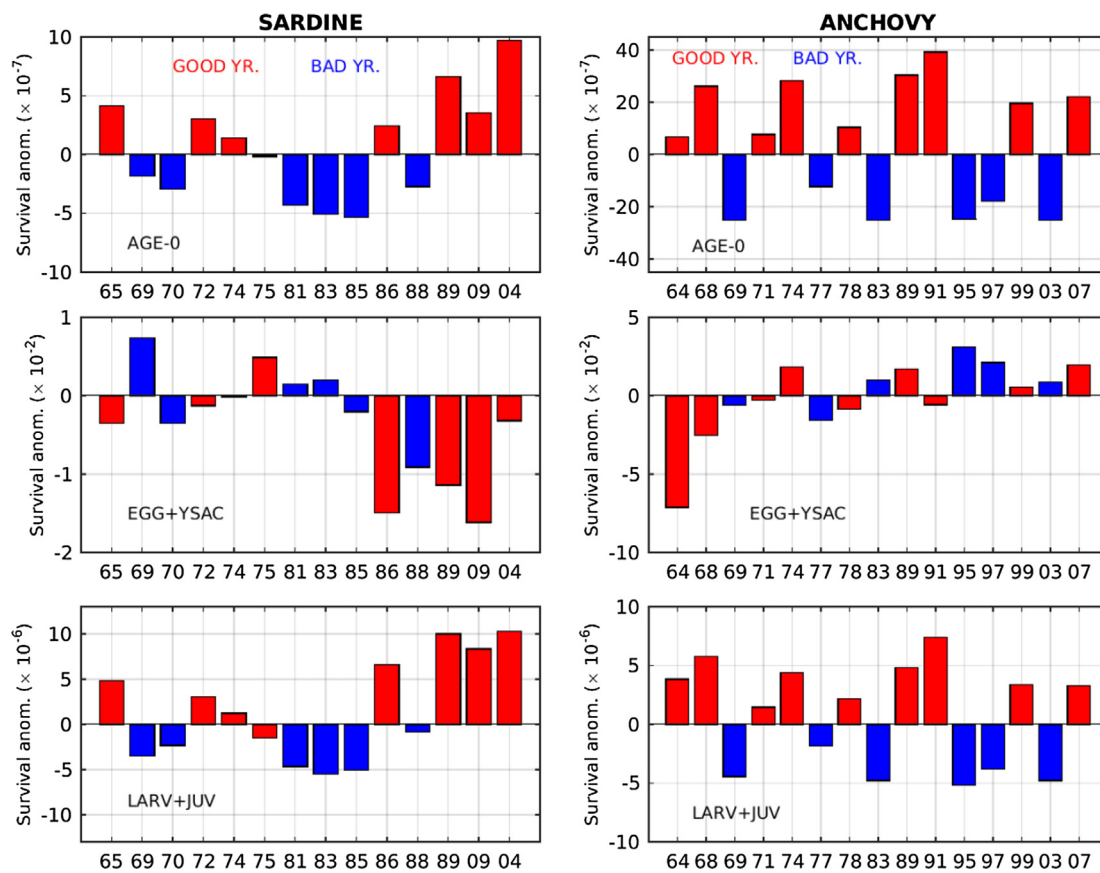


Fig. 14. Survival anomaly of age-0 (eggs to juveniles; top), non-feeding age-0 (eggs + yolk-sacs; middle), and feeding age-0 (larvae + juveniles; bottom) individuals during good and bad years for sardine (left) and anchovy (right) in the historical simulation. Anomalies for good and bad years are represented with red and blue colour bars respectively. Survival rate from life stage  $s_1$  to  $s_2$  is the number of individuals exiting stage  $s_2$  divided by number of individuals entering stage  $s_1$ . Anomalies refer to deviation with respect to the 1964–2007 mean. (For interpretation of the references to colour in this figure legend, the reader is referred to the web version of this article.)

CanCS among major eastern boundary upwelling ecosystems. The results also point to noticeable differences in the spatial distributions between sardine and anchovy. Anchovy appear largely restricted to the northern shelf of Morocco, while sardine extend across a much broader region of the CanCS. While the overall distribution of sardines is supported by estimates from acoustic surveys (Aristegui et al., 2009), there are no consistent observations supporting nor rejecting the spatial distribution simulated for anchovy. However, a possible issue for anchovy is the misidentification of a southern stock between Cape Verde and Cape Blanc, where the model yields a minor fraction of the total anchovy biomass (Fig. 9m–p). This result is not supported by the non-negligible landings off Mauritania and Senegal (not shown). An explanation for this discrepancy, and potential caveat to model results, is that the CanCS is sufficiently broad to host different stocks with different biological traits. For instance, it is known that the southern subpopulations become more tolerant to warmer temperatures and that the onset and duration of the spawning season can change from one habitat to another. The chosen biological traits for anchovy and sardine to use in the model, particularly optimum temperature, were representative of the central part of the CanCS domain (from Cape Blanc

to the Strait of Gibraltar), the area sustaining most of the fish biomass. Hence, it is plausible that the IBM, as configured here, is not adequately representing the secondary southernmost and Iberian stocks.

Simulated variability in the sardine and anchovy adult biomasses shows a decadal-scale response qualitatively similar to that suggested by the landings, used here as a proxy of the actual population biomass. Given the significant uncertainties of this proxy and in our knowledge of the fish bioenergetics and behaviour as modelled herein (see R15 for discussion), a rigorous quantitative validation of the model (e.g., correlation of predicted versus observed) is not warranted at this stage of model development. Instead, the analyses reported here had two main purposes. The first is a demonstration that the R15 model can be ported to another upwelling system (i.e., the CanCS), and with relatively minor changes to parameter values, the modelling approach can capture decadal cycles of sardine and anchovy characteristic of the new system. With the successful development of this new version, the second purpose was to shed light on the causes for interannual and decadal variability of sardine and anchovy in the CanCS.

While uncertainties remain, a major result of the CanCS version is that sardine and anchovy biomasses vary concurrently, a behaviour that

Table 2

Pearson correlation coefficient between  $\Delta p$  and eggs/ind, and between  $\Delta p$  and age-0 survival over anomalous years in the historical simulation. Only the subset of model results corresponding to good and bad years were included in the correlations. Coefficients with asterisks are statistically significant at 95% confidence level.

	#Eggs/ind (age-2)	#Eggs/ind (age-3)	Survival age-0	Survival egg + ysac	Survival lrv + juv
$\Delta p$ (sardine)	0.75*	0.72*	0.84*	-0.50	0.86*
$\Delta p$ (anchovy)	0.44	0.38	0.93*	-0.29	0.95*

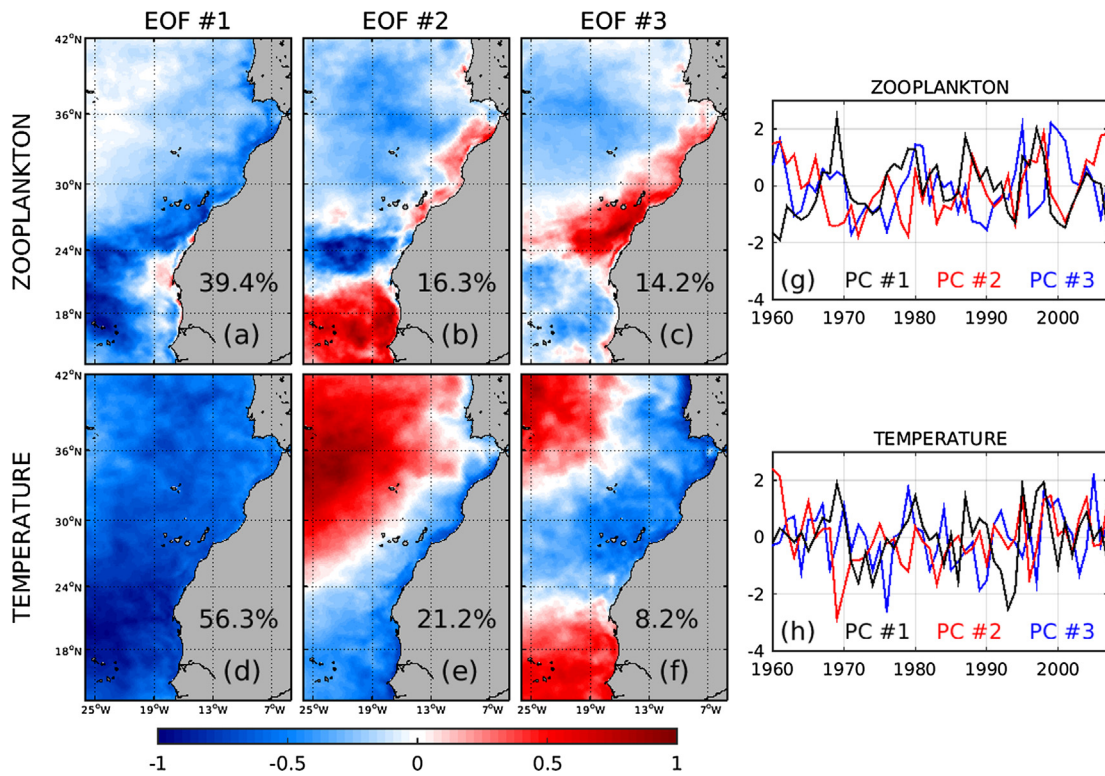


Fig. 15. First three EOF modes for surface zooplankton (a–c) and SST (d–f). Modes were normalized by their corresponding maximum absolute values. The EOF analysis was applied to yearly zooplankton (ZS + ZL + ZP) and SST series derived from the historical simulation outputs. The percentage of the total variance explained by each mode is labelled. Right panels: first three principal components (standardized) for surface zooplankton (g) and temperature (h).

differs from the analogous simulation of R15 for the northern anchovy and Pacific sardine in the California Current. A first analysis reveals that this synchronous variability stems from the combination of one biological factor and one environmental factor: the common reliance of sardine and anchovy on food and the concomitant interannual variability of zooplankton (as well as temperature) over the main sardine and anchovy habitats. This finding suggests that sardine and anchovy in the CanCS both respond primarily to overall food abundance, whereas in the California Current simulation they were affected more by local food and temperature conditions. Fiechter et al. (2015) found that sardine in the California Current was particularly sensitive to SST changes (via survival of eggs and yolk-sac stages), while anchovy responded to food availability (via egg production). Because food and temperature are two environmental properties that normally oscillate in opposite phase, good periods for sardine were typically poor for anchovy and vice versa. In our results for the CanCS, this mechanism is

not at play because of the smaller role played by local SST conditions in differentially affecting sardine and anchovy population dynamics. One possible explanation for lack of species differences related to temperature is that the CanCS experiences significantly warmer temperatures than the California Current (~19 °C versus ~15 °C), making egg and yolk-sac development time less sensitive to SST fluctuations – the slope of the development time curve decreases with temperature (Eq. (1)). Reduced variation in egg and yolk-sac development times implies more consistent mortality rates and stage survivals, and therefore a smaller role of ocean temperatures in driving the variability age-0 survival in the CanCS. This explanation for synchrony in the CanCS generated by the model simulation requires more investigation and additional simulations (e.g., sensitivity analysis) for confirmation.

Although both sardine and anchovy vary according to food availability in the historical simulation, stronger winds are not always better, which links our simulation results to the optimal environmental

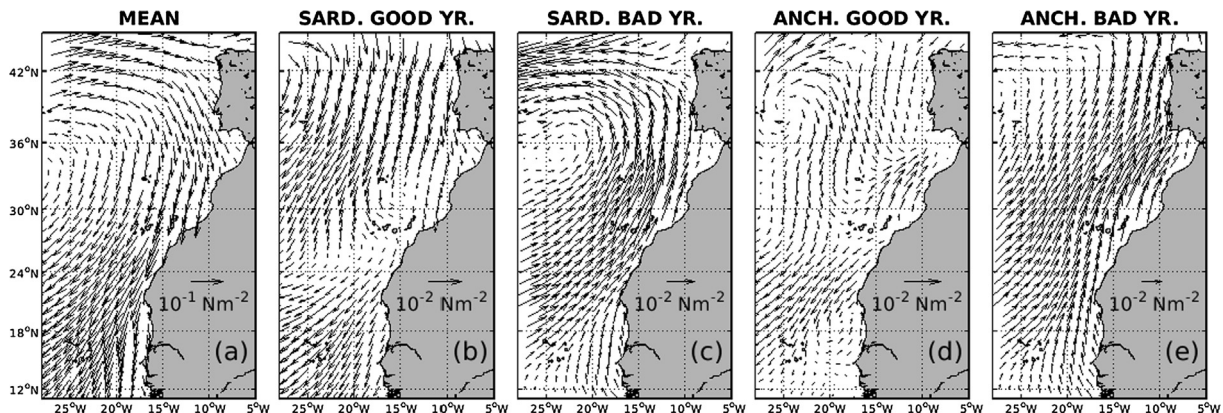
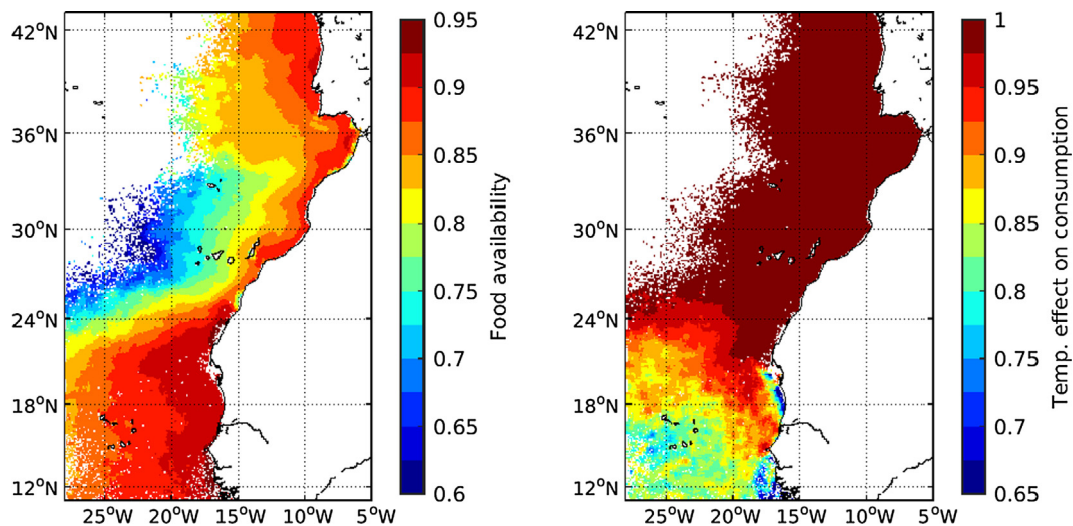


Fig. 16. Mean surface wind stress during the historical simulation (a) and averaged anomalies during good and bad years for sardine and anchovy (b–e). From left to right: (b) good years for sardine; (c) bad years for sardine; (d) good years for anchovy; (d) and bad years for anchovy.



**Fig. 17.** Mean food availability (left;  $P$ -value, Eq. (2)) and temperature effect on consumption experienced by anchovy larvae (right) in the historical simulation. The two magnitudes are non-dimensional. Greater values imply more favourable conditions for larvae survival.

window hypothesis suggested for upwelling ecosystems (Cury and Roy, 1989). In fact, larval mortality associated with enhanced southward advection (downstream with respect to the coastal upwelling jet) emerges as the main process constraining anchovy recruitment in the simulation. Further, while sardine also do not benefit from extreme upwelling and advection, the resulting effect in the simulation is much weaker than for anchovy.

Our analysis provides a first step towards the use of end-to-end modelling to decipher the underlying biological and environmental factors that affect sardine and anchovy in the CanCS. Based on the historical simulation, key biological processes were identified by focusing on anomalously good and bad years in terms of annual changes of adult population abundance. A next step would be to follow Fiechter et al. (2015) and apply a lagged correlation analysis to the entire simulation time period to identify cause-effect relationships between size of the adult population, yearly egg production and survival of age-0 individuals. Such an analysis would allow to better discern the relative contribution of egg production versus age-0 survival in driving the interannual variability of sardine. Other analyses could focus on documenting the apparent minor role played by temperature in differentially affecting sardine and anchovy, perhaps by using the conditions experienced by individuals (Lagrangian) over time, and the inclusion of fishery and harvest in the model. Finally, a correlation-based analysis of the model results with modes of climate variability would enable a “climate-to-fish” linkage. A notable influence of the North Atlantic Oscillations (NAO), the first mode of atmospheric variability in the North Atlantic, is expected. A positive NAO index is associated with stronger winds and upwelling in the CanCS (Visbeck et al., 2003) and hence, according to our results, sardine and anchovy would generally thrive under a positive NAO phase. However, since anchovy require more moderate upwelling than sardine, their response to the NAO will likely not be equal. It is plausible for sardine and anchovy to be most tightly connected with different (but not totally independent) climate modes, despite both species tending to fluctuate synchronously.

We will continue the analysis of the CanCS version of the model and move towards using the two versions of the R15 model in a comparative mode (Megrey et al., 2009). Given our first insights into the synchronous variability of sardine and anchovy in the CanCS, a detailed comparison to the asynchronous response identified for the California Current is warranted. The changes needed to adapt the California Current version of the model to the CanCS were relatively small and thus our results show that the end-to-end model can generate both types of behaviour as they emerge from the physics, NPZ and seemingly small

differences between sardine and anchovy attributes. A comparison between the historical simulations for the California Current and CanCS, and hopefully other systems, specifically designed to allow side-by-side comparisons (e.g., same analyses of the outputs in both systems, same definitions of good and bad years, etc.) would allow for robust inferences about the how environmental and biological conditions affect sardine and anchovy population dynamics.

#### Acknowledgements

J.C.S.-G. was supported by a “Juan de la Cierva” postdoctoral grant (JCI-2012-13451) from the Spanish Ministry of Economy, Industry and Competitiveness. This work was initiated during a visit at the NOAA/NMFS Southwest Fisheries Science Center in San Diego, funded by a “José Castillejo” mobility grant from the Spanish Ministry of Education, Culture and Sport. We thank Evan Mason for valuable discussions on the ROMS implementation in the CanCS. The model calculations were carried out in the facilities of the Supercomputing and Bioinnovation Center of the University of Malaga.

#### Appendix A. Supplementary material

Supplementary data to this article can be found online at <https://doi.org/10.1016/j.pcean.2018.12.009>.

#### References

- Alheit, J., Roy, C., Kifani, S., 2009. Decadal-scale variability in populations. In: Checkley, D., Alheit, J., Oozeki, Y., Roy, C. (Eds.), *Climate Change and Small Pelagic Fish*. Cambridge University Press, New York, pp. 64–87.
- Amante, C., Eakins, B.W., 2009. ETOPO1 1 Arc-Minute Global Relief Model: Procedures, Data Sources and Analysis. NOAA Technical Memorandum NESDIS NGDC-24. National Geophysical Data Center, NOAA. doi:10.7289/V5C8276M.
- Aristegui, J., Barton, E.D., Tett, P., Montero, M.F., García-Muñoz, M., Basterretxea, G., Cussatlegras, A.-S., Ojeda, A., de Armas, D., 2004. Variability in plankton community structure, metabolism, and vertical carbon fluxes along an upwelling filament (Cape Juby, NW Africa). *Prog. Oceanogr.* 62, 95–113.
- Aristegui, J., Álvarez-Salgado, X.A., Barton, E.D., Figueiras, F.G., Hernández-León, S., Roy, C., Santos, A.M.P., 2006. Oceanography and fisheries of the Canary Current Iberian region of the Eastern North Atlantic. In: In: Robinson, A., Brink, K.H. (Eds.), *The Global Coastal Ocean: Interdisciplinary Regional Studies and Syntheses, The Sea: Ideas and Observations on Progress in the Study of the Seas*, vol. 14. Harvard University Press, pp. 877–931.
- Aristegui, J., Barton, E.D., Álvarez-Salgado, X.A., Santos, A.M., Figueiras, F.G., Kifani, S., Hernández-León, S., Mason, E., Machú, E., Demarcq, H., 2009. Sub-regional ecosystem variability in the Canary Current upwelling. *Prog. Oceanogr.* 83, 33–48.
- Baddy, M., Guénette, S., 2002. The Fisheries off the Atlantic Coast of Morocco 1950–1997. In: Zeller, D., Watson, R., Pauly, D., (Eds.), *Fisheries Impacts on North*

- Atlantic Ecosystems: Catch, Effort and National/Regional Data Sets. vol. 9(3). Univ. British Columbia, Vancouver, pp. 191–205. Fisheries Centre Research Reports.
- Bakun, A., 1996. Patterns in the Ocean: Ocean Processes and Marine Population Dynamics. University of California Sea Grant, San Diego.
- Barange, M., Bernal, M., Cercole, M.C., Cubillos, L., Cunningham, C.L., Daskalov, G.M., De Oliveira, J.A.A., Dickey-Collas, M., Hill, K., Jacobson, L., Køster, F.W., Mase, J., Nishida, H., Niquen, M., Oozeki, Y., Palomera, I., Saccardo, S.A., Santojanni, A., Serra, R., Somarakis, S., Stratoudakis, Y., van der Lingen, C.D., Uriarte, A., Yatsu, A., 2009. Current trends in the assessment and management of small pelagic fish stocks. In: Checkley, D., Alheit, J., Oozeki, Y., Roy, C. (Eds.), *Climate Change and Small Pelagic Fish Stocks*. Cambridge University Press, Cambridge.
- Barton, E., 1998. Eastern boundary of the North Atlantic: Northwest Africa and Iberia. Coastal segment (18, E). In: In: Robinson, A., Brink, K.H. (Eds.), *The Sea*, vol. 11. John Wiley & Sons Inc., pp. 633–657.
- Baumgartner, T.R., Soutar, A., Ferreira-Bartrina, V., 1992. Reconstruction of the history of Pacific sardine and northern anchovy populations over the past two millennia from sediments of the Santa Barbara Basin, California. *California Cooper. Fish. Investigat. Rep.* 33, 24–40.
- Belvéze, M., Boerema, L.K., Azzou, M.M., El Belghiti, M.A., 1980. Report of the Second Meeting of the Working Group on Sardine (*Sardina pilchardus* Walb.), FAO CECAF/ECAF Ser. 79/15.
- Belvéze, M.H., Erzini, K., 1983. The influence of hydro-climatic factors on the availability of the sardine (*Sardina pilchardus* Walbaum) in the Moroccan Atlantic fishery. *FAO Fisher. Rep.* 291, 285–328.
- Bernal, M., Jiménez, M.P., Duarte, J., 2011. Anchovy egg development in the Gulf of Cádiz and its comparison with development rates in the Bay of Biscay. *Fisher. Res. – FISH RES.* 117. <https://doi.org/10.1016/j.fishres.2011.04.010>.
- Binet, D., 1988. Rôle possible d'une intensification des alizés sur le changement de répartition des sardines et sardinelles de long de la côte ouest-africaine. *Aquat. Living Resour.* 1, 115–132.
- Blaxter, J.H.S., Hunter, J.R., 1982. The biology of the clupeoid fishes. In: In: Blaxter, J.H.S., Russell, F.S., Yonge, M. (Eds.), *Advances in Marine Biology*, vol. 20. Academic, London, pp. 1–223.
- Bravo de Laguna, J., Fernández, M.A.R., Santana, J.C., 1976. The Spanish fishery on sardine (*Sardina pilchardus*) off West Africa. *ICES. C. M.* 1976/J:13.
- Brochier, T., Auger, P.A., Pecquerie, L., Machu, E., Capet, X., Thiaw, M., Mbaye, B.C., Cheikh-Baye, B., Omar, E., Charouki, N., Sene, O.N., Werner, F., Brehmer, P., 2018. Complex small pelagic fish population patterns arising from individual behavioral responses to their environment. *Prog. Oceanogr.* 164, 12–27.
- Carton, J.A., Giese, B.S., 2008. A reanalysis of ocean climate using Simple Ocean Data Assimilation (SODA). *Mon. Weather Rev.* 136, 2999–3017.
- Chapman, D.C., 1985. Numerical treatment of cross-shelf open boundaries in a barotropic coastal ocean model. *J. Phys. Oceanogr.* 15, 1060–1075.
- Checkley, D., Alheit, J., Oozeki, Y., Roy, C., 2010. *Climate Change and Small Pelagic Fish Stocks*. Cambridge University Press, Cambridge, pp. 64–87 382, [Doi: 10.1111/j.1475-4959.2010.00360.2.x](https://doi.org/10.1111/j.1475-4959.2010.00360.2.x).
- Checkley, D., Rebecca, G.A., Rykaczewski, R.R., 2017. Climate, anchovy, and sardine. *Annu. Rev. Mar. Sci.* 9, 469–493.
- Conkright, M.E., Boyer, T.P., 2002. *World Ocean Atlas 2001: Objective Analyses, Data Statistics, and Figures*. CD-ROM Documentation, National Oceanographic Data Center, Silver Spring, MD, pp. 17.
- Coombs, S., Smyth, T., Conway, D.V.P., Halliday, N.C., Bernal, M., Stratoudakis, Y., Álvarez-del-Pozo, J.P., 2006. Spawning season and temperature relationships for sardine (*Sardina pilchardus*) in the eastern North Atlantic. *J. Mar. Biol. Ass. U.K.* 86, 1245–1252.
- Cury, P., Roy, C., 1989. Optimal environmental window and pelagic fish recruitment success in upwelling area. *Com. J. Fish Aquat. Sci.* 46, 670–680.
- Donlon, C.J., Martin, M., Stark, J., Roberts-Jones, J., Fiedler, E., Wimmer, W., 2012. The operational sea surface temperature and sea ice analysis (OSTIA) system. *Remote Sens. Environ.* 116, 140–158.
- Ganias, K., Somarakis, S., Nunes, C., 2014. Reproductive potential. In: Ganias, K. (Ed.), *Biology and Ecology of Sardines and Anchovies*. CRC Press, Boca Raton, FL, pp. 79–121.
- García-Muñoz, M., Aristegui, J., Pelegrí, J.L., Antoranz, A., Ojeda, A., Torres, M., 2005. Exchange of carbon by an upwelling filament off C. Ghir (NW Africa). *J. Mar. Syst.* 54, 83–95.
- Garrido, S., van der Lingen, C.D., 2014. Feeding biology and ecology. In: Ganias, K. (Ed.), *Biology and Ecology of Sardines and Anchovies*. CRC Press, Boca Raton, FL, pp. 122–189.
- FAO, 2001. Report of the FAO working group on the assessment of small pelagic fish off Northwest Africa. *FAO Fisheries Report No.* 657, p. 133.
- FAO, 2012. Report of the FAO working group on the assessment of small pelagic fish off Northwest Africa. *FAO Fisheries and Aquaculture Report No.* 1036, p. 245.
- Fiechter, J., Rose, K., Curchitser, E.N., Hedstrom, K.S., 2015. The role of environmental controls in determining sardine and anchovy population cycles in the California Current: analysis of an end-to-end model. *Prog. Oceanogr.* 138, 381–398.
- Flather, R.A., 1976. A tidal model of the north-west European continental shelf. *Mem. Soc. R. Sci. Liège* 6 (10), 141–164.
- Fréon, P., Curry, P., Shannon, L., Roy, C., 2005. Sustainable exploitation of small pelagic fish stocks challenged by environmental and ecosystem changes: a review. *Bull. Mar. Sci.* 76, 38–462.
- Fréon, P., Barange, M., Aristegui, J., 2009. Eastern boundary upwelling ecosystems: integrative and comparative approaches. *Prog. Oceanogr.* 83, 1–14.
- Fulton, E.A., 2010. Approaches to end-to-end ecosystem models. *J. Mar. Syst.* 81 (1–2), 171–183.
- Fulton, E.A., Link, J.S., Kaplan, I.C., Savina-Rolland, M., Johnson, P., Ainsworth, C., Horne, P., Gorton, R., Gamble, R.J., Smith, A.D.M., Smith, D.C., 2011. Lessons in modelling and management of marine ecosystems: the Atlantis experience. *Fish. Fish.* 12, 171–188.
- Holzlohner, S., 1975. On the recent stock development of *Sardina pilchardus* Walbaum off Spanish Sahara. *ICES C.M.* 1975/J: 13ICES 2000. Report of the Working Group on the Assessment of Mackerel, Horse Mackerel, Sardine, and Anchovy (WGMHSA). *ICES CM 2000/ACFM:05*, p. 546.
- Humston, R., Olson, D.B., Ault, J.S., 2004. Behavioral assumptions in models of fish movement and their influence on population dynamics. *Trans. Am. Fish. Soc.* 133 (6), 1304–1328.
- ICES, 2014. Report of the Working Group on Southern Horse Mackerel, Anchovy and Sardine (WGHANSA), 20–25 June 2014, Copenhagen, Denmark. *ICES CM 2014/ACOM:16*, p. 599.
- ICES, 2015. Report of the Working Group on Southern Horse Mackerel, Anchovy and Sardine (WGHANSA), 24–29 June 2015, Lisbon, Portugal. *ICES CM 2015/ACOM:16*, p. 612.
- ICES, 2016a. Report of the Working Group on Southern Horse Mackerel, Anchovy and Sardine (WGHANSA), 24–29 June 2016, Lorient, France. *ICES CM 2016/ACOM:17*, p. 588.
- ICES, 2016b. EU request to ICES on in-year advice for anchovy (*Engraulis encrasicolus*) in Division 9.a (Atlantic Iberian waters). In Report of the ICES Advisory Committee, 2016. *ICES Advice 2016, Book 7, Section 7.4.1*. ICES Special Request Advice.
- ICES, 2017. Report of the Workshop on Age estimation of European anchovy (*Engraulis encrasicolus*). *WKARA2 2016 Report 28 November - 2 December 2016*. Pasaia, Spain. *ICES CM 2016/SSGIEOM:17*, p. 223.
- Johnson, T.B., Evans, D.O., 1991. Behavior, energetics, and associated mortality of young-of-the-year white perch (*Morone americana*) and yellow perch (*Perca flavescens*) under simulated winter conditions. *Can. J. Fish Aquat. Sci.* 48, 672–680.
- Kifani, S., 1998. Climate dependant fluctuations of the Moroccan sardine and their impact on fisheries. In: Durand, M.H., Cury, P., Mendelsohn, R., Roy, C., Bakun, A., Pauly, D. (Eds.), *Global Versus Local Changes in Upwelling Systems*. ORSTOM Editions, Paris, pp. 235–248.
- Kishi, M.J., Ito, S., Megrey, B.A., Rose, K.A., Werner, F.E., 2011. A review of the NEMURO and NEMURO.FISH models and their application to marine ecosystem investigations. *J. Oceanogr.* 67, 3–16.
- Kishi, M.J., Kashiwai, M., Ware, D.M., Megrey, B.A., Eslinger, D.L., Werner, F.E., Aita-Noguchi, M., Azumaya, T., Fujii, M., Hashimoto, S., Huang, D., Iizumi, H., Ishida, Y., Kang, S., Kantakov, G.A., Kim, H.-C., Komatsu, K., Navrotsky, V.V., Smith, L.S., Tdokoro, K., Tsuda, A., Yamamura, O., Yamanaka, Y., Yokouchi, K., Yoshie, N., Zhang, J., Zuenko, Y.I., Zvansky, V.I., 2007. NEMURO – introduction to a lower trophic level model for the North Pacific marine ecosystem. *Ecol. Model.* 202, 12–25.
- Large, W.G., Yeager, S.G., 2008. The global climatology of an interannually varying air–sea flux data set. *Clim. Dyn.* 33, 341–363.
- Large, W.G., McWilliams, J.C., Doney, S.C., 1994. Oceanic vertical mixing: a review and a model with a vertical K-profile boundary layer parameterization. *Rev. Geophys.* 32 (4), 363–403.
- Letcher, B.H., Rice, J.A., Crowder, L.B., Rose, K.A., 1996. Variability in survival of larval fishes: disentangling components of variance with a generalized individual-based model. *Can. J. Fish Aquat. Sci.* 53, 787–801.
- Lluch-Belda, D., Crawford, R.J.M., Kawasaki, T., MacCall, A.D., Parrish, R.H., Schwartzlose, R.A., Smith, P.E., 1989. World-wide fluctuations of sardine and anchovy stocks: the regime problem. *S. Afr. J. Mar. Sci.* 8 (1), 195–205.
- Mason, E., Colas, F., Molemaker, J., Shchepetkin, A.F., Troupin, C., McWilliams, J.C., Sangrà, P., 2011. Seasonal variability of the Canary Current: a numerical study. *J. Geophys. Res.* 116, C06001. <https://doi.org/10.1029/2010JC006665>.
- Megrey, B.A., Rose, K.A., Klumb, R.A., Hay, D.E., Werner, F.E., Eslinger, D.L., Smith, S.L., 2007. A bioenergetics-based population dynamics model of Pacific herring (*Clupea harengus pallasii*) coupled to a lower trophic level nutrient–phytoplankton–zooplankton model: description, calibration, and sensitivity analysis. *Ecol. Model.* 202, 144–164.
- Megrey, B.A., Link, J.S., Hunt Jr, G.L., Moksness, E., 2009. Comparative marine ecosystem analysis: applications, opportunities, and lessons learned. *Prog. Oceanogr.* 81 (1–4), 2–9.
- Millan, M., 1999. Reproductive characteristics and condition status of anchovy *Engraulis encrasicolus* L. from the bay of Cadiz (SW Spain). *Fish. Res.* 41, 73–86.
- Motos, L.A., 1996. Reproductive biology and fecundity of the Bay of Biscay anchovy population (*Engraulis encrasicolus* L.). *Sci. Mar.* 60 (Suppl. 2), 195–207.
- Platt, T., Gallegos, C.L., Harrison, W.G., 1980. Photoinhibition of photosynthesis in natural assemblages of marine phytoplankton. *J. Mar. Res.* 38, 687–701.
- Rose, K.A., Rutherford, E.S., McDermott, D., Forney, J.L., Mills, E.L., 1999a. Individual based model of walleye and yellow perch populations in Oneida Lake. *Ecol. Monogr.* 69, 127–154.
- Rose, K.A., Cowan, J.H., Clark, M.E., Houde, E.D., Wang, S.B., 1999b. An individual based model of bay anchovy population dynamics in the mesohaline region of Chesapeake Bay. *Mar. Ecol. Prog. Ser.* 185, 113–132.
- Rose, K.A., Allen, J.I., Artioli, Y., Barange, M., Blackford, J., Carlotti, F., Cropp, R., Daewel, U., Edwards, K., Flynn, K., Hill, S.L., HilleRisLambers, R., Huse, G., Mackinson, S., Megrey, B., Moll, A., Rivkin, R., Salihoglu, B., Schrum, C., Shannon, L., Shin, Y.J., Smith, S.L., Smith, C., Solidoro, C., St. John, M., Zhou, M., 2010. End-to-end models for the analysis of marine ecosystems: challenges, issues, and next steps. *Mar. Coast. Fish.* 2, 115–130.
- Rose, K.A., Fiechter, J., Curchitser, E.N., Hedstrom, K., Bernal, M., Creekmore, S., Haynie, A., Ito, S., Lluch-Cota, S., Megrey, B.A., Edwards, C.A., Checkley, D., Koslow, T., McClatchie, S., Werner, F., MacCall, A., Agostini, V., 2015. Demonstration of a fully-coupled end-to-end model for small pelagic fish using sardine and anchovy in the California Current. *Prog. Oceanogr.* 138, 348–380.

- Sammartino, S., García Lafuente, J., Naranjo, C., Sánchez-Garrido, J.C., Sánchez Leal, R., Sánchez Román, A., 2015. Ten years of marine current measurements in Espartel Sill, Strait of Gibraltar. *J. Geophys. Res. Oceans* 120, 6309–6328. <https://doi.org/10.1002/2014JC010674>.
- SeaWiFS Project, 2003. SeaWiFS Global Monthly Mapped 9 km Chlorophyll-a. Ver. 1. PO. DAAC, CA, USA.
- Salvatteci, R., Field, D., Gutiérrez, D., Baumgartner, T., Ferreira, V., Ortlieb, L., Sifeddine, A., Grados, D., Bertrand, A., 2018. Multifarious anchovy and sardine regimes in the Humboldt Current System during the last 150 years. *Glob. Change Biol.* 24, 1055–1068.
- Scheffer, M., Baveco, J.M., DeAngelis, D.L., Rose, K.A., van Nes, E.H., 1995. Superindividuals a simple solution for modelling large populations on an individual basis. *Ecol. Model.* 80, 161–170.
- Schwartzlose, R.A., Alheit, J., Bakun, A., Baumgartner, T., Cloete, R., Crawford, R.J.M., Fletcher, W.J., Green-Ruiz, Y., Hagen, E., Kawasaki, T., Lluch-Belda, D., Lluch-Cota, S.E., MacCall, A.D., Matsuura, Y., Nevarez-Martinez, M.O., Parrish, R.H., Roy, C., Serra, R., Shust, K.V., Ward, N.M., Zuzunaga, J.Z., 1999. Worldwide large-scale fluctuations of sardine and anchovy populations. *South Afric. J. Mar. Sci.* 21, 289–347.
- Shchepetkin, A.F., McWilliams, J.C., 2005. The regional oceanic modeling system (ROMS): a split-explicit, free-surface, topography-following-coordinate oceanic model. *Ocean Model.* 9, 347–404.
- Takasuka, A., Oozeki, Y., Kubota, H., Lluch-Cota, S.E., 2008. Contrasting spawning temperature optima: why are anchovy and sardine regime shifts synchronous across the North Pacific? *Prog. Oceanogr.* 77 (2–3), 225–232.
- Travers, M., Shin, Y.-J., Jennings, S., Cury, P., 2007. Towards end-to-end models for investigating the effects of climate and fishing in marine ecosystems. *Prog. Oceanogr.* 75, 751–770.
- Visbeck, M., Chassignet, E.P., Curry, R.G., Delworth, T.L., Dickson, R.R., Krahnmann, G., 2003. The Ocean's response to North Atlantic oscillation variability. In: Hurrell, J.W., Kushnir, Y., Ottersen, G., Visbeck, M. (Eds.), *The North Atlantic Oscillation: Climatic Significance and Environmental Impact*. American Geophysical Union, Washington D.C. <https://doi.org/10.1029/134GM06>.
- Watkins, K.S., Rose, K.A., 2013. Evaluating the performance of individual-based animal movement models in novel environments. *Ecol. Model.* 250, 214–234.
- Werner, F.E., Ito, S., Megrey, B.A., Michio, J., Kishi, M.J., 2007. Synthesis of the NEMURO model studies and future directions of marine ecosystem modeling. *Ecol. Model.* 202, 211–223.
- Winemiller, K.O., Rose, K.A., 1992. Patterns of life-history diversification in North American fishes: implications for population regulation. *Can. J. Fish. Aquat. Sci.* 49 (10), 2196–2218.
- Zweifel, J.R., Lasker, R., 1976. Prehatch and posthatch growth of fishes—a general model. *Fish. Bull.* 74, 609–621.